Available online at www.sciencedirect.com

SCIENCE @ DIRECT®

ELSEVIER

Coordination Chemistry Reviews 248 (2004) 1421–1446

COORDINATION CHEMISTRY REVIEWS

www.elsevier.com/locate/ccr

Review

Counter-electrode function in nanocrystalline photoelectrochemical cell configurations

N. Papageorgiou*

Laboratory of Photonics and Interfaces, Swiss Federal Institute of Technology, CH–1015 Lausanne, Switzerland

Received 10 October 2003; accepted 9 March 2004
Available online 20 July 2004

Contents

Abstract

The search for rigid or flexible photoelectrochemical solar cell counter-electrode (CE) alternatives has been a continuous effort and long ongoing process in our lab, as studies in CE kinetic performance and stability on the one hand seek to improve the overall efficiency of the solar cell,

---

* Tel.: +41 21 6936129; fax: +41 21 6934111.
E-mail address: nicholas.pappas@epfl.ch (N. Papageorgiou).

0010-8545/$ – see front matter
doi:10.1016/j.ccr.2004.03.028

while attempting to adapt to novel design concepts or new materials, on the other. The dye-sensitized TiO_2 nanocrystalline solar cell utilizing the iodide/tri-iodide redox mediator served as the system of reference for a theoretical characterization and computational simulation used to scrutinize CE performance, which was coupled by experimental exploration of catalyst materials and different design options. Two basic approaches can be identified with respect to CE design. Firstly, there is the case where the catalyst has sufficient kinetic performance and can be utilized when deposited on any stable support material current collector even at monolayer quantities, and secondly, the case when the kinetics of the catalyst are insufficiently high to sustain the required currents and therefore the effective exchange current density must be enhanced by internal surface area increase, thus the need to impart porosity to either the catalyst material or the current collector or both. The kinetic/electrocatalytic performance of candidate catalyst materials, as well as the mass-transfer limitations of commonly applied cell configurations have been determined in most cases by means of experiment. However, predictions have also been made by electrochemical simulation of a variety of given systems under steady-state operation, where the CE is examined as an integral part of the energy conversion system, making clear the implications of the varying physical and geometric parameters of the comprising elements of the device, i.e. the porous photoelectrode, the spacer configuration and the CE, including also the nature and the properties of the electrolyte constituting their junction.

Keywords: Mass-transport; Redox mediator; Nanocrystalline PEC; Counter-electrode; Solar cell model

1. Introduction

PECs work on a different principle than conventional solid-state solar cells, whereby the processes of light absorption and charge separation are differentiated. One of the important characteristics of the liquid junction photovoltaic cell is that photogenerated charge separation takes place at the interface of the semiconductor in contact with an ionically conducting electrolyte containing a suitable redox charge mediator that should, after electron injection into the semiconductor conduction band, effectively perform the function of shuttling the generated positive charge away from the light absorbing sensitizer residing on the semiconductor surface, (usually a transition metal complex, the molecular properties of which are specifically engineered for the task) to the CE, thus completing the electrical circuit (see Fig. 1). Via this last electron transfer at the CE, in which the mediator is returned to its reduced state, the circuit is closed, finally resulting in a net direct current passing from photoelectrode to the CE within the cell itself and from CE to photoelectrode in the external circuit of the device under illumination.

The theoretical maximum voltage that such a device could deliver corresponds to the difference between the redox potential of the mediator and the Fermi level of the semiconductor and can only be achieved on open circuit, i.e. at zero current. Under load, however, the CE potential is less than on open circuit, due to losses incurred by the passage of current through the electrolyte, i.e. the mass-transfer overpotential, as well as the same current conveyed through the electrolyte/CE interface, i.e. the kinetic overpotential. The electrolyte ionic conductivity and the mediator species transport from one electrode to the other are the fundamental parameters determining the magnitude of the potential loss described as mass-transfer overpotential (η_{mt}), whereas the electrocatalytic properties of the CE surface towards mediator reduction will determine the magnitude of the potential loss referred as kinetic or charge-transfer overpotential (η_{ct}). The total voltage loss at the CE is the sum of the above, represented in Fig. 1 by the overall CE overpotential (η_{CE}).

As well as studying the effect of the electrocatalytic properties of the CE materials themselves, the following sections explore the influence of the design component physical parameters of the photoelectrochemical system and thus attempt to quantify their effects on the overall performance of the solar cell. Inasmuch as the function of the CE consists in the effective regeneration of the oxidized state of the electrolyte mediator to its reduced—in addition to the efficient supply of this reduced state of the mediator towards the photoelectrode where it will undertake the ‘interception’ of the oxidized sensitizer, thus regenerating its ground state in order to perpetuate the operation cycle-the properties of the electrolyte such as conductivity, viscosity, the reduced and oxidized mediator mass-transport and their diffusivities within the mesoporous elements and the cell bulk electrolyte as a function of the nature of the support electrolyte have also been studied in the context of overall solar cell performance. All the above effects are analyzed and compared in order to reflect their repercussions with respect to optimal cell performance and efficiency.

1.1. Part I. The kinetic overpotential

1.1.1. Mediator reduction materials and electrocatalyst optimization

The electrodic reduction of iodine from solutions containing the iodide/iodine or iodide/poly-iodide redox couple in aqueous as well as organic solvent media, has attracted much attention for its fundamental interest to electrochemists studying the mechanism and the reaction kinetics of the system, and for its practical significance in applications such as photoelectrochemical solar cells. Previous literature indicates that the iodine/tri-iodide reduction reaction is not reversible on all materials indiscriminently, this including Pt. The kinetics are solvent dependent, being most facile in water [1–3] and acetonitrile [3–5] and increasingly more sluggish in DMSO [6], DMF [5], propylene carbonate [3,5,7–9], as evidenced by the wide variation of exchange current densities reported on smooth platinum cathodes,

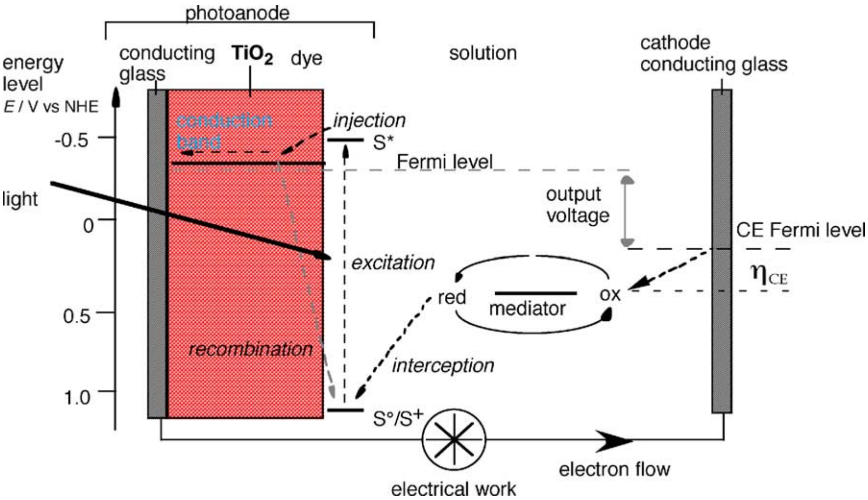

Fig. 1. Light absorption is performed by a monolayer of dye (S) adsorbed chemically at the semiconductor surface. After having been excited by a photon, it is able to transfer an electron to the semiconductor (the process of "injection"), while the electric field inside the bulk material allows extraction of the electron. Positive charge is transferred from the dye (S^+) to a redox mediator ("interception") present in the solution with which the cell is filled, and thence to the CE.

which extends over three or four orders of magnitude. Accurate quantitative comparison remains difficult as the concentrations, choice of cations, supporting electrolytes used etc., vary from author to author. Nonetheless, much research effort has been dedicated to understanding the irreversible electrochemical behavior of the iodine/tri-iodide reduction reaction. There are indications of blocking iodine layers on electrodes [10], of the spontaneous oxidative chemisorption of iodide as iodine atoms on noble metal surfaces [11], as well as non-electroactive adsorbed iodide and/or iodine [12] have been proposed in the literature.

Transparent CEs based on conducting tin (cto) or indium tin oxides (ito), are widely used to minimize the losses due to mass-transport of the redox relay species in large surface area photoelectrochemical cells. In aqueous and organic polyiodide electrolytes, the above CEs exhibit very slow electron-transfer kinetics which leads to substantial power losses in such devices. The cto and ito presently used as cathodes in photoelectrochemical solar energy devices are extremely poor catalysts for iodine reduction, and have therefore been modified, mainly by means of transition metal electro-deposition or radiolytic grafting of metal nano-aggregates onto their surface [13–16], thus enhancing iodine reduction kinetics in aqueous sytems.

Dye-sensitized nanocrystalline solar cells based on regenerative photoelectrochemical principles [17,18] utilize the iodide/tri-iodide redox couple as the mediator that shuttles the charge between the site of sensitizer regeneration on the photoelectrode to the CE. During the mediator regenerative cycle, the oxidized species, namely iodine or tri-iodide, must be converted back (reduced) to iodide, according to reaction $I_3^- + 2e = 3I^-$, at minimum energy loss on the CE. In view of the use of organic electrolytes and room temperature molten salts in current solar energy conversion systems [19,20], there has been an imminent need to minimize the energy losses around the maximum power point—due to a low fill-factor—as well as the performance limitations imposed on the system by iodine reduction, thus, posing much higher demands on the electrocatalytic properties of the CE. As will be analyzed in the following sections, thermally produced nano-sized platinum metal clusters have succeeded in overcoming the above mentioned catalytic limitations.

Another scope in these studies was to explore CE alternatives, e.g. for flexible PEC solar cells. However, the application of the catalyst is limited so far to the substrates that can withstand the high temperature preparation conditions required. The heating stage of the catalyst formation (385 °C) is tolerated by F-doped SnO_2-coated glass surfaces or layered graphite sheets, but not so well by, e.g. polymer based laminated surfaces, which may exhibit low sheet resistance at room temperature, though will warp or oxidize when heated. Therefore, a low temperature catalyst preparation is indispensable to the promotion of other substrates as candidates for the further development of solar cells of particular characteristics or of broader design/construction options.

Under a recent development project, the desire to impart flexibility to the solar panel, has led to significant modifications of the materials comprising the photoelectrode: the mesoporous TiO_2 layer was deposited on Ti metal sheet. This obviously obstructs the photoelectrode side illumination of the cell, which should now be back-side illuminated. In turn, the success of the CE illumination mode rests on the very low optical absorbance of the CE in the useful range of the spectrum combined with sufficiently high tri-iodide reduction kinetics and finally the long-term performance stability of the electrode. The above challenges formed the objectives of this work. Moreover, flexible Pt and Ti/Pt-sputtered polymer based sheets were envisaged for use as CE and were tested for kinetic performance without any treatment or conditioning in organic solar cell electrolytes.

In order to fulfill the requirements of low temperature surface catalyzation, CE flexibility, in addition to transparency (minimum absorbance of the solar spectrum by the CE for back-side illumination cell development), conducting polymer laminated flexible as well as transparent sheets have been surface catalyzed by Pedot, using a variety of preparation techniques/conditions and were subsequently tested for their kinetics performance under electrochemically controlled conditions, in addition to applied as CE in experimental sealed and open solar cell performance tests. Pedot and the Pedot/Pss water dispersion commercial product also found novel applications in CE fabrication; solar cell tests were conducted with Pedot electrochemical preparations on cto or other cast surfaces, and graphite/Pedot/Pss composite pastes were developed with very low sheet resistance, intending to solve limitations due to the series resistance, kinetic resistance and low temperature production, by casting the CE directly on the prepared photoelectrode plate.

2. Experimental

2.1. Chemicals—electrochemical techniques

Cto was fluorine-doped, with square resistance of 10 Ω, 5% haze, supplied by Libbey-Owens-Ford Co., Ohio, USA. Ito glass of square resistance 8 Ω, supplied by Flachglas Germany. Ruthenium oxide electrodes were fabricated by multilayer thermal decomposition of $RuCl_3$ ethanolic solution, at 500 °C. The graphite electrodes were type Papyex, supplied by Carbon Lorraine, France. Electrodes of sputtered platinum on glass were prepared on our site. Solvents used were acetonitrile (Fluka puriss), propylene carbonate (Burdick & Jackson, high purity). *N*-methyl-oxazolidine-2-one (NMO) (1.5 kg) was distilled from barium oxide (200 g, Fluka) (95 °C, 4 Pa), then distilled again from phosphorus pentoxide (180 g, Fluka) (95 °C, 4 Pa). The synthesis of the organic iodide salts methyl-ethyl-morpholinium iodide, MEMI and methyl-hexyl-imidazolium iodide, MHImI, employed herein has been described elsewhere [21]. Tetrabutyl-ammonium iodide, TBAI (Fluka puriss) was used as supplied. Pedot (poly-3,4 ethylenedioxythiothene) was prepared via the electropolymerization of the Edot monomer, and Pedot/Pss (polystyrenesulfonate anion doping) 50% dispersion in water where both Bayer research products. Electrolytes employed the above solvents with the addition of organic iodide salts and iodine at concentrations reflecting the present requirements of the nanocrystalline solar cell, typically 500 and 50 mM, respectively.

Electrochemical impedance spectroscopy was employed on symmetric thin-layer cells, similar to the ones described elsewhere [20], in order to determine the kinetic performance of the electrodes. The charge-transfer resistance R_{ct} value of the electrode under study, was taken as the half of the real component of the impedance, which appears as the semicircle at the high frequency end of the spectrum [22]. The Autolab P20 potentiostat of Ecochemie, equipped with frequency response analysis was used. Electrochemical platinization of conducting tin oxide glass was carried out by cathodic polarization at approximately 2 mA/cm^2 in aqueous hexachloroplatinic acid solution (ca. 0.15 M). Platinum loadings were determined by dissolution of the electrodes in aqua regia and platinum content in the subsequent diluted solutions measured by ICP atomic emission spectroscopy. Electrochemical preparation of Pedot was done using the Edot monomer solution (10 mM) in AcN and in the presence of 0.1 M EMIm-imide as electrolyte. Cyclic voltammetry and chrono-coulometry were applied to produce the electropolymerization of Edot. The thermal platinum nano-cluster catalyst, i.e. the electrode preparation method for the catalytic electrochemical reduction of iodine/tri-iodide in organic media, is described elsewhere [37]. Another method for the preparation of the catalytic electrode was through an organic ligand (tetrabutylammonium) stabilized platinum cluster (e.g. crystallite size ca. 6 nm) solution [23] used to coat the conducting electrode substrate, and the solvent medium dried off under vacuum at 150 °C and then heated in air for 12 h to 300–350 °C (removal of organic ligand).

3. Discussion

The required performance characteristics of the CE are determined by the maximum current delivered by the solar cell under short circuit conditions, which present nanocrystalline photoanode technology sets at 20 mA/cm^2 [19]. Considering a tolerance for the voltage loss on the CE as being <10 mV, one arrives at a $R_{ct} < 0.5\,\Omega\,cm^2$ threshold for the charge-transfer resistance. This value corresponds to an exchange current density $J_o > 2.6 \times 10^{-2}$ A/cm^2 on the basis of the formula $R_{ct} = RT/nFJ_o$, which assumes the linear approximation of the current-overpotential equation, where $n = 2$ for reaction $I_3^- + 2e = 3I^-$. In the case of, e.g. NMO taken as the model electrolyte solvent, electrochemically deposited Pt on cto is below CE performance requirements, by one to two orders of magnitude for economically viable Pt metal loadings, i.e. acceptable price to performance ratio.

Moreover, chemical stability studies under prolonged anodic polarization in the same as above chemical environment were conducted. Electro-deposited Pt is prone to dissolution or anodic corrosion in the presence of iodide, which technically results in detrimental effects on overall solar cell performance and long-term stability. This fact also alludes to the possibility of Pt dissolution even under open circuit conditions. Either way, introduction of Pt in any form of compound or charged complex will always impair solar module performance on all power output levels, ranging from mW/cm^2 to the sub-μW applications. In practice, mechanical rigidity and stability of the CE against abrasion or generally mechanical contact is a desired property, and

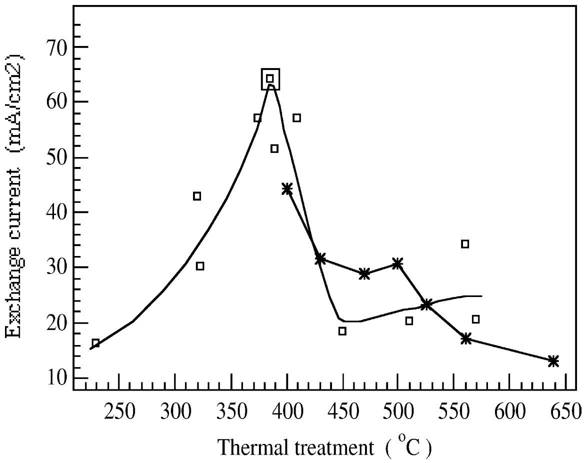

Fig. 2. Dependence of exchange current density on thermalization temperature for the platinum thermal cluster catalyst on cto glass. Electrolyte 0.42 M methyl-ethyl-morpholinium iodide and 50 mM I_2 in NMO. Pt loading 2 μg/cm^2.

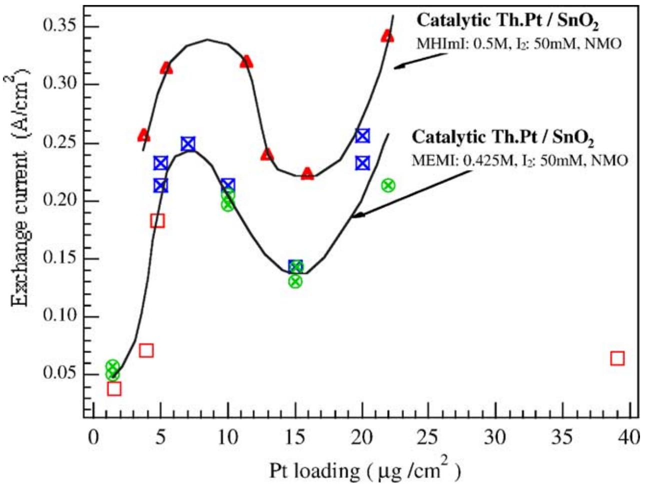

Fig. 3. Variation of exchange current density with platinum loading for the platinum thermal cluster electrocatalyst on a tin-oxide substrate and for two different electrolytes.

in this respect electroplatinized electrodes have proven to be very poor as well.

3.1. The thermal platinum nano-cluster catalyst

This particular thermal preparation method described above for Pt deposition creates a catalytic interface solely composed of Pt metal and probably not involving other chemical elements such as chloride or carbonateous material, as evidenced by ESCA analysis. However, the presence of physi- and chemi-sorbed oxygen has not been excluded, as certain publications claim oxygen sorption at elevated temperatures [24], others pure dioxide formation by the thermal decomposition [25,26] etc. A strong metal-support interaction involving an interaction with the elements of the cto electrode substrate [27], may be contributing also for the substrates studied, but no direct evidence of the presence of substrate elements on platinum could be found. However, the performance generally, from the comparison with the other substrates described in Section 2, does not appear to be dependent on the substrate chosen. This catalyst overcomes all the above mentioned disadvantages and limitations in regards to tri-iodide reduction kinetic performance, in addition to offering electrochemical/chemical stability and mechanical durability of the CE.

The catalyst preparation procedure was optimized in terms of final curing temperature, taken as the only variable parameter and all others considered constant, for the reduction kinetics of tri-iodide on cto in organic electrolytes (Fig. 2). It was observed that, independent of platinum loading, and in a reproducible manner, there exists a rather narrow temperature region where the exchange current is maximized and an exclusive point (ca. 385 °C) where the exchange current appears reproducibly at its maximum value and without the slightest indication of deterioration of these kinetics in the medium to long term, when operating as cathode. Other temperatures produce electrodes that appear to 'drift' from an initial value and tend to irreversibly stabilize in the short term at lower exchange current values. The plot in Fig. 3 indicates the kinetic performance of the thermally produced catalyst. The exchange current density on the thermal catalyst exceeds by almost an order of magnitude the desired kinetic performance characteristics of a solar cell CE, for the most 'deactivating' solvent NMO. In fact, calculating on the basis of 0.184 A/cm^2 exchange current (minimum performance of the thermal catalyst at 5 μg/cm^2), we find $R_{ct} = 0.07\,\Omega\,cm^2$, which is interpreted as a loss of merely 1.4 mV at 20 mA/cm^2 during solar cell operation. The galvanic or electrochemical Pt on the same cto glass, i.e. same roughness factor, and at the same Pt loading exhibits a charge-transfer resistance of 7.6 Ω cm^2, incurring a voltage loss of 152 mV at 20 mA/cm^2. This is certainly a modification of kinetics on the molecular level, i.e. electrocatalysis, and not an artifact of enhanced electrode effective surface etc., as can be directly interpreted from the experimental evidence in Table 1, where the same bright Pt and thermal catalytic Pt electrodes were used in three different solvents. The ratio of the exchange current values would have simply been a constant if it were an effect of surface area alone. However, these results reveal a solvent dependent improvement of up to 250 times of the electrocatalytic properties of the electrode treated with thermal catalyst.

Table 1
Exchange current densities measured on bright Pt and thermal Pt cluster on conducting tin oxide for different solvents

Solvent	$J_{o,galv}$ (mA/cm^2)	$J_{o,catal}$ (mA/cm^2)	Ratio
AcN	71	350	5
PC	2.25	184	82
NMO	0.75	183	243

Electrolytes contained MEMI: 0.425 M, I_2: 50 mM.

The variation of exchange current with iodide and iodine concentrations, with all other electrolyte parameters kept constant, provides significant information on the mechanism of a multistep reaction [28,29]. Comparison of electro-deposited platinum and thermal platinum cluster on cto in the same solutions of TBAI in propylene carbonate, indicated a difference in reaction mechanism or the effect on the cation for the two electrode types.

The effective surface area of the thermal platinum surfaces were compared with smooth platinum by hydrogen adsorption and oxide formation coulometry in aqueous solution [30], and confirmed that the platinum surface area approximately corresponds to a monolayer on the cto substrate. The low Pt loadings required on these electrodes (e.g. $5\,\mu g/cm^2$ of Pt on a surface with a roughness factor of 3, corresponding to a one monolayer Pt coverage of the support), render them optically transparent electrodes (OTEs). At this point it is also important to emphasize the selectivity aspect with respect to other reactions, as the above catalyst for iodine reduction proved to be an inhibitor for bromine reduction.

The catalytic CE, regardless of the preparation method can be described as follows: the catalyst is structurally characterized as nano-sized, pure platinum metal naked crystalline clusters or micro-crystallites, i.e. developed crystallites with exposed crystal or lattice planes, clearly visible under HR-TEM. These platinum nanocrystallites are microscopically polyhedral toward spherical in geometry, and are sparsely dispersed over the electrode substrate surface, the rest of the substrate being devoid of platinum, that is to say, there is no detectable platinum aside from the crystalline particles on the electrode surface (same analysis on an electro-deposited sample found Pt on the entire surface). High resolution electron microscopy (HRTEM) with EDX-analysis was applied to study the microstructure of the surface of the CE. Images of particles taken from the surface of the electrode prepared by electro-deposition of Pt did not reveal the widespread presence of clearly identifiable distinct Pt-particles, although upon close inspection lattice fringes could be detected in this area indicating thin Pt sheets. Apparently, this electrode had either very small Pt-particles (<1 nm) or thin Pt films on the electrode surface. The thermally prepared electrode image on the other hand, shows only distinct Pt-nanoparticles on the surface of the cto. Fig. 4 top frame shows a representative cto particle with four Pt-particles. Selected area EDX-analyses confirmed the Pt-nature of these particles. In Fig. 4 middle image, the region with the Pt particles is magnified and this further magnification shows a distinct large Pt particle with lattice fringe resolution, surrounded by large cto crystals. Fig. 4 bottom frame shows the high resolution image documenting the crystalline nature of the Pt. Selected area EDX-analyses of other particle areas show no detectable Pt. The Pt on this electrode is present in the form of rather large Pt-clusters several nm in diameter.

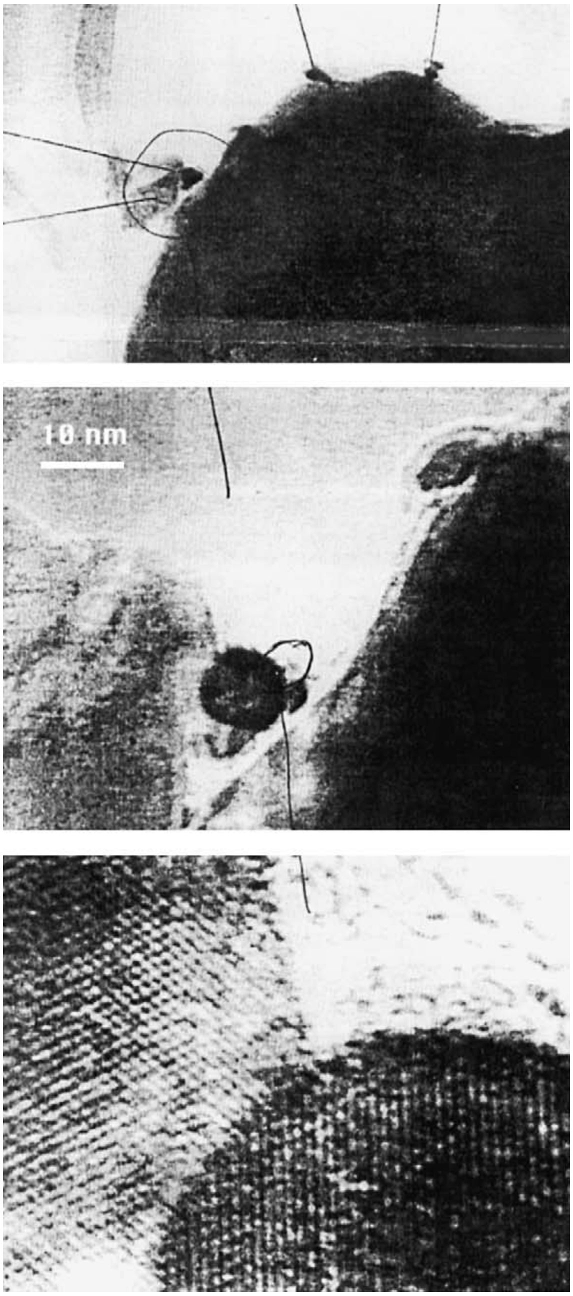

Fig. 4. HRTEM micrographs obtained of particles from the surface of the CE prepared by impregnation and thermal decomposition. The micrograph frames are successive magnifications of a single area. The Pt-nature of the large particle in the bottom image was confirmed by selected area EDX.

The size of the crystalline clusters covers a large range below approximately 20 nm in diameter, the maximum performance most likely appearing for a size distribution centered around 5 nm. The role of the exact size of the clusters is not yet understood, other than the economy possible the smaller the Pt particles. That is to say, crystallite size and loading are inter-related for optimum kinetic performance and desired electrode transparency. The optimum size could very well be a function of the operating organic solvent, and therefore rendering the catalyst specific to the type of organic solvent. The unexpected decrease trend with increasing loading seen in graph Fig. 3 is an effect of the change

Table 2
Various porous materials as potential CEs for a nanocrystalline solar cell

Electrode/material	$R_{\mathrm{ct,eff}}$ ($\Omega\,\mathrm{cm}^2$)	$i_{\mathrm{o,eff}}$ ($\mathrm{mA/cm}^2$)
Porous carbon, 50 μm (80% graphite, 20% carbon black) [14]	12–20	1.07–0.64
Graphite paper (∼200 μm) (Papyex “N”, Carbone Lorraine)	350–300	0.037–0.043
Nanotubes on graphite paper [15]	200–250	0.064–0.051
Ru oxide, CVD layer, 50–100 nm[a]	∼1000	0.012
Colloidal RuO_2 film, 50 μm (50% porosity)[a]	∼20	∼0.64
Screen-printed Pt layer (∼20 $\mu\mathrm{g/cm}^2$)[a]	5–10	1.3–2.6
Pt cluster catalyst (5 $\mu\mathrm{g/cm}^2$)	0.06	200

Electrocatalytic properties have been measured according to the previously described electrochemical impedance method. Acetonitrile used as solvent may be reduce further the R_{ct}.

[a] Own preparation.

in average particle size formed during preparation and thus of decreasing exposed surface. At even higher loadings the effective surface area increase appears to dominate, rather than the size. The specific temperature regime carried out on the electrode during the catalyst preparation procedure may be related to surface adsorbed or bonded light elements, e.g. oxygen in the catalytic interface could be a key factor for this behavior, but recrystallization is very likely to be taking place as well on the platinum particles.

Moreover, a comparative kinetic evaluation of certain active material catalyst alternatives, mostly of the enhanced surface area or porous type seen below in Table 2., makes more apparent the advantages of the thermal Pt catalyst.

3.2. Flexible sputtered Pt/polymer sheet CE testing for catalytic activity

For increased accuracy of the kinetic measurements, a multiply reused thermal cluster catalyst on cto served as the electrode of reference for kinetic performance comparisons. The above described impedance technique gave an average value of $1.75\,\Omega\,\mathrm{cm}^2$ for the kinetic resistance per electrode in the organic electrolyte. The corresponding value for the sputtered Pt on polymer laminate received (unspecified) varied between 3.6 and $5.0\,\Omega\,\mathrm{cm}^2$. The electrocatalysis evaluation experiments were conducted under the same conditions as the thermal reference sample and no surface preparation, rinsing, polarization or electrochemical conditioning was performed on the test samples. A second set of electrodes prepared and specified as alternate multilayer coatings of 5–10 Å of sputtered Pt and Ti metal, were designated Pt5A, Pt5ATi5A and Pt10ATi5A, their name denoting the structure of the deposit. The recorded kinetic resistance values were as follows: Pt5A: 6.2, Pt5ATi5A: 5.3 and Pt10ATi5A: $14.5\,\Omega\,\mathrm{cm}^2$. It is noteworthy that the refreshing of the electrolyte in the thin-layer test cell produced lower kinetic resistance for the series as, e.g. for the case of Pt10ATi5A, 14.5 initially decreased to 7.5 in a subsequent run of the same test. This phenomenon may also suggest that a chemical surface pretreatment involving iodide or even pure organic solvent could substantially improve the as received catalytic performance of such layer preparations.

3.3. Surface catalysis by electrochemical Pedot deposition

The first attempts to catalyze the rigid cto surface with electrochemically prepared Pedot consisted in the in situ electropolymerization of the Edot monomer in organic solution. The working cto electrode was cycled between 0.5 and 2 V AgCl and the gradual build up of the blue surface coating was observed. The de-doping of the conducting doped material was observed at −0.4 V thus verifying the doped (and less colored) state of the produced deposits. This method produced blue colored electrode surfaces with poor mechanical strength, albeit with reasonable catalytic activity ($4\,\Omega\,\mathrm{cm}^2$) as also confirmed by the feedback from solar cell *I–V* test data. The uniformity of the deposit was not always good and unclean cto surfaces were very prone to incomplete coatings and blemishes. Additionally, the control of the Pedot loading was not possible at low levels and therefore unsuitable for the preparation of transparent layers. In conclusion, the dendritic growth of the Pedot resulted in poor adhesion to the substrate and the total Pedot mass had a considerably low dispersion over the surface, thus reducing the strength and the quality of the catalyst.

Transparent coatings were produced using a pulse technique, such as chrono-coulometry for very short times, i.e. below 1 s, e.g. 0.3 s at 5–10 $\mathrm{mA/cm}^2$ could produce light coatings that were acceptable in terms of absorbance as well as in kinetic performance in sealed cell tests. These catalyst depositions could be done on any flexible electrode supplied with ease and reproducibility. The independent impedance evaluation of week old deposits gave 4–5 $\Omega\,\mathrm{cm}^2$ depending on the loading. It was also observed that freshly made electrodes had better performance in the solar cell ($<3\,\Omega\,\mathrm{cm}^2$ by impedance). The pulse deposition improved markedly the mechanical strength of the layer and its resistance to abrasion. However, there are still lingering questions regarding the longer term stability of this successful performance. It must be said that although the operational potential of the

CE within the solar cell (ca. 0.1 V AgCl) is far enough positive with respect to the de-doping limit of the material, thus avoiding the direct electrochemical de-doping to the non-conducting state, Pedot has been reported as being able to form charge-transfer complexes with iodine. Similarly interesting in terms of kinetic performance, Pedot surface activated 'carbon paper' (Papyex, Carbone Lorraine) electrodes were produced for solar CE tests, which could combine the very low sheet resistance (1 Ω/square). Large surface cto (>5 cm^2) CE was prepared with a Pedot activated surface in a specially adapted three electrode electrochemical cell along with other smaller CEs, this time distinguished by a significant blue coloration, yet transparent in order to counteract the dye coloration, for a final transparent blue effect of the solar panel.

3.4. Graphite/Pedot/Pss composite electrodes

Commercial product Pedot/Pss was used to prepare light blue coatings on cto (of a maximum few microns thickness) in order to conduct experiments for tri-iodide catalysis, combining transparency and chemical stability (insolubility in contact with solar electrolytes). Though the mechanical properties of these coating are superb and the stability sufficient, the surface is not a catalyst for the reduction of tri-iodide, and the resistance of the coated electrode unexpectedly increases, although the product forms conducting layers when dried. The conductivity is apparently too low in this case, thus adding to the total series resistance.

On the other hand, the product was viewed as a binder for composite electrode preparation with an increased internal surface and lower sheet resistance, towards the development of conducting graphite pastes for solar cell CE production. This was envisaged as a low temperature method for directly depositing a CE over the finished photoelectrode that would not require further heating after the casting. This CE deposition would not impair the flexibility of the photoelectrode either as it should inherently have a significant degree of flexibility as well, to follow the photoelectrode bending. Graphite 10 μm powder was mixed with Pedot/Pss liquid product until a very viscous consistency paste was formed. This paste could then be cast onto cto or even on insulating slides and left to dry. The sheet resistance of the resulting 40–60 μm layer was 4 Ω in the best case. The layer sheet resistance was similar when deposited on insulating glass. The great advantage of the lower resistance had to be combined now with the catalytic activity of the electrochemical Pedot, as the untreated layer did not perform well in a solar cell. The Pedot activated layer presented shunting problems when assembled with a photoelectrode, which proved to be the result of blisters formed on the CE after some time in the presence of the solar electrolyte. Graphite swelling is the most plausible explanation. Eventually the layer increased its resistance and the structural integrity of the electrode was compromised.

4. Conclusion

In view of the use of organic electrolytes in solar energy conversion systems, and the imminent need to minimize the energy efficiency losses and the performance limitations imposed on the system by iodine reduction on the CE, a catalyst was developed. The specific temperature regime and procedure described for the thermal decomposition of platinum-chloride (platinum-bromide or possibly other Pt compounds) from anhydrous isopropanol (or possibly other organic solvents), produces an electrode interface that is a selective catalyst for iodine/tri-iodide reduction in organic electrolytes, matching the kinetics reported in aqueous iodide/iodine systems. This technology produces catalytic electrodes that are electrochemically/chemically stable in their operating environment, in addition to providing superior mechanical endurance or robustness, good adherence to substrate The catalyst has been structurally characterized as nano-sized platinum metal clusters. The very low platinum loadings (less than 3 μg/cm^2), render these electrodes optically transparent and economy in the quantity of platinum used is an additional advantage. The technology can be applied to all solar energy conversion systems utilizing the iodide/tri-iodide redox couple as mediator or any iodide/tri-iodide mediated electrochemical device.

The specific platinum deposition procedure and temperature regime carried out for the thermal decomposition of platinum-chloride precursors from anhydrous isopropanol, produces a surface phase or catalytic interface structurally defined as nano-sized platinum crystallites, in form of clusters, that is a selective catalyst for iodine/tri-iodide reduction, presenting unprecedented kinetic performance in organic media, matching only that of reported aqueous iodide/iodine systems. The kinetic performance of a PEC cell CE (i.e. exchange current of the tri-iodide reaction) is of the essence with respect to the voltage consumed to maintain the counter-electrode process. Conventional methods produce CE exhibiting very slow electron transfer kinetics for tri-iodide reduction, which are dependent on the type of organic solvent in the organic solvent electrolytes and on the solute iodide salt cation within. It has been demonstrated that electrochemically deposited Pt on cto does not produce electrodes capable of reducing iodine (or tri-iodide in organic media) without severe losses in potential and the fill-factor of the solar cell, thus limiting its performance. The above problem appears increasingly so as one uses solvents other than acetonitrile as the cell electrolyte, e.g. nitroethane, propylene and ethylene carbonate, *n*-methyl-pyrrolidone (NMP), *n*-methyl-oxazolidinone (NMO) etc. The introduction of room temperature molten salt systems as electrolytes in these devices either diluted with the above solvents or neat, poses higher demands on counter-electrode performance.

Hence, a catalyst has been developed, which can be applied on these substrates to provide: (i) extremely superior kinetic performance, as compared to the reported literature or solar cell practice (two to four orders of magnitude higher exchange currents), (ii) chemical/electrochemical stability in practical cells (no corrosion or dissolution which results in photoelectrode deactivation), (iii) very low cost counter-electrodes (low loading). (iv) mechanically stable and robust counter-electrode surfaces (handling ease). (v) optical transparency combined with high kinetic performance for the counter-electrode. These qualities have proven to be the result of a modification of kinetics on the molecular/mechanism level, i.e. electrocatalysis, by which the detrimental effects on the electrode reaction of the solvent molecule, the supporting cation or/and iodide related species and the employed chemical additives in the solar cell are suppressed, and is therefore not an artifact of enhanced electrode effective surface, increased dispersion etc. Furthermore, the novel electrocatalytic properties of platinum thermal clusters are likely to find applications for other chemical systems in the general area of catalysis, photocatalysis and electrocatalysis. The technology can be applied to all solar energy conversion systems utilizing iodide/tri-iodide redox couple as mediator, sensor devices or any iodide/tri-iodide mediated electrochemical device.

4.1. Part II. The mass-transfer overpotential

4.1.1. Mediator transport in multilayer nanocrystalline photoelectrochemical cell configurations

The dye-sensitized TiO_2 nanocrystalline solar cell utilizing the iodide/tri-iodide redox mediator served as the system of reference for a theoretical characterization and computational simulation used to scrutinize its performance when viewed as an integral system incorporating a porous CE and a porous spacer layer in between. The concentration profiles of the redox mediator of the thin-layer solar cell, as well as the concentration (mass-transfer) overpotential established on the CE and the limiting current of the cell are affected by the addition of a separation layer between the electrodes and by the geometric and structural properties of the CE itself. Numerical solutions could be obtained from the mathematical model simulating the system that can explain the behavior observed in experimental cells. The feasibility of the porous CE as an alternative is discussed through the model predictions and the experimental kinetic performance data of candidate materials.

Interesting concepts on liquid junction photovoltaic cell optimization have been previously developed by Orazem and Newman [31], where the relation of cell design parameters and power output performance was explored. Among other things, these authors demonstrate and quantify the influence of the positioning of the CE relative to the semiconductor–electrolyte interface, with reference to mass-transfer and kinetic limitations, the electrolyte resistance and the important role they play in the optimal design of the liquid junction photovoltaic cell. In a previous publication, the redox mediator function in thin layer nanocrystalline photoelectrochemical solar cells operating under steady state illumination has been examined, in terms of the mass-transfer processes of the species involved [32]. With reference to the nanocrystalline TiO_2 photoelectrode, a number of simplified models of this type of cell were developed, which provided a significant degree of understanding of the effect of various factors on their operation. There, the influence of certain solar cell parameters on its operation was explored and the optimum iodide and tri-iodide concentrations in the cell electrolyte was obtained, taking into account various restrictions these are subject to. Also investigated were the conditions under which the mass-transfer overpotential loss can impair the I versus V characteristic of a nanocrystalline photoelectrode coupled with a planar catalytic CE, resulting in a decreased fill-factor (ff) values. Different light absorption modes within the cell were envisaged. The overall energy output efficiency (η_{eff}) of the photoelectrochemical cell can be limited by the voltage losses incurred by the CE process, and on the other hand by the local iodide concentration that for reasons at present not well understood is critical for efficient sensitizer regeneration in the photon to current conversion cycle, and therefore, such phenomena understandably have consequences on the power ultimately delivered by the device.

In a broader approach the aim would be to further investigate the influence of an alternative CE design and cell configuration on the above mentioned performance characteristics, by assuming the photoelectrode layer parameters are constant. It seems reasonable to consider in situations where the CE kinetics are poor or limiting that an increase in the effective exchange current can be achieved by simply increasing the effective surface area of the CE material. This implies that the dimension along the x-axis would have to increase as well. On the other hand, electrically insulating layers acting also as scattered light back diffusers may be necessary to incorporate between the CE and the photoelectrode in order to decrease shunt losses or even increase light absorption of the device, which adds also to the total length, thus affecting mass transport. The physical characteristics of each cell section, such as porosity and thickness, and the mass transport characteristics in the liquid, such as diffusion coefficients and their effective values as they are determined by the structure of the porous solid phase in the bicontinuous phase network, are taken into consideration in a mathematical mass-transfer model simulating the behavior of the complete cell at the steady-state. Efficient design characteristics for such cells can be envisaged in order to minimize, e.g. the mass-transfer overpotential, thus minimizing one of the sources of loss in such cells, as well as ensuring the optimum conditions for efficient charge injection, minimum power loss due to dark current and photon absorption by the tri-iodide. The repercussions of the variation of solar cell design parameters are illustrated experimentally by the performance of practical application devices.

As an analytical solution was not possible, a numerical approach was implemented, giving accurate numerical solutions to the system of equations and boundary conditions constituting a mass-transfer model for the more general multilayer cell configuration. The above cell simulation can predict the local concentrations of the electroactive species (iodide and tri-iodide), in order to judge whether the cell and electrolyte design are optimal, and therefore be able to determine the operational limits of the given electrode–spacer–electrolyte configuration. A monochromatic light irradiation is assumed, corresponding to the absorption maximum (540 nm) of the experimental sensitizer *cis*-$(SCN^-)_2$ bis(2,2′-bipyridyl-4,4′-dicarboxylate) ruthenium(II) [19] without damage to the generality of white light illumination with respect to the trends observed.

5. Problem formulation

5.1. Cell description

In order to avoid the difficulties inherent to a complete model of such a cell, due to the complexity of the behavior of the colloidal semiconductor medium from a charge-transfer and charge transport point of view, and of the effects taking place at the liquid solid TiO_2 interface and throughout, the problem is confined here to the effect of mass transport of the various ionic species present between and within the two electrodes in the liquid, i.e. in the pores of the porous materials. Migrational or double layer effects have not been considered here as conditions applied can be replicated that render these influences negligible [20,32]. The CE is taken to be composed of a conducting material, and thus ohmic losses are negligible on passage of current along the *x*-axis. A middle layer positioned between the photoelectrode and the CE, called henceforth spacer, is assumed to be a perfect electronic insulator and structurally of a mesoporous nature. A schematic representation of the cell is given in Fig. 5.

Under steady state operation, the concentrations of the ionic species are independent of time but depend on a single coordinate, *x*, perpendicular to the cell electrodes. The intensity of the illumination, assumed to be in the *x* direction and from the photoelectrode side, affects the species concentration, which are also affected by the current density delivered by the device. When current passes through the cell, the steady state concentrations of the mediator redox couple (I^-/I_3^-) are space dependent and different from the initial or open circuit concentrations. The corresponding concentration potential loss, the mass-transfer overpotential, is quantitatively determined here. When the photon flux irradiating the cell becomes sufficiently large, and the electric load appropriate, the maximum current density that can be obtained eventually becomes limited by the mass transport of the species to values that we also determine. The physical size of the cell, the thickness of the layers affect its performance. Quantitative evaluations as well as experimental evidence for these effects have been obtained.

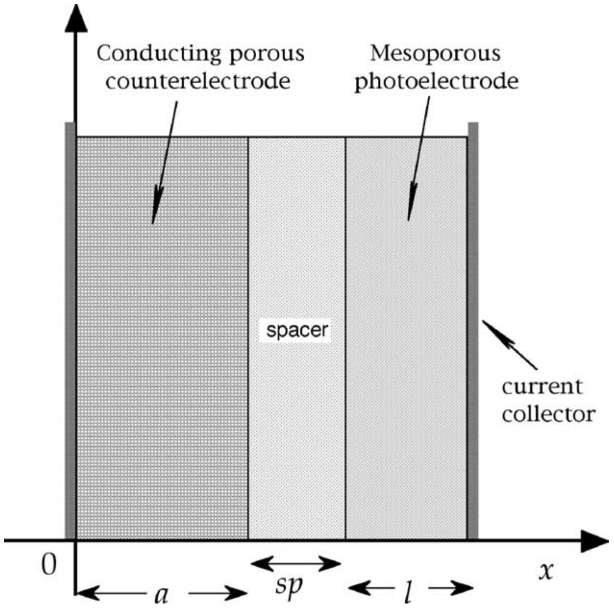

Fig. 5. Schematic representation of a thin layer nanocrystalline photoelectrochemical cell. Illumination is provided from the photoelectrode side.

The light absorbing dye is adsorbed on some porous semiconductor (e.g. TiO_2) which operates as the anode (electrode on right in Fig. 5). It has a typical thickness, *l*, of the order of 10 μm. It is deposited on a conducting substrate, generally conducting tin oxide (CTO) covered glass. A spacer layer is in contact with the photoanode (to its right) and with the conducting CE porous layer (to its left). Both of these layers have thicknesses that are also adjusted and are typically of the order of 10–100 μm. The cathode should have appropriate properties to catalyze the reduction of I_3^-. Moreover, the intrinsic exchange current density for tri-iodide reduction on the CE material is also an adjustable system parameter in the simulation. The complete mathematical formulation of the model is described elsewhere [32].

The CE behavior can be mathematically simplified by considering the CE material as an ideal electronic conductor and as such taken as an equipotential surface under steady state examined here. This premise damages very little the generality of the model as this requirement of very low ohmic loss across the layer is expected in a practical CE material. Due to the μm order thickness of a CE, ohmic drop in the normal direction at the current densities anticipated is much less than the electrochemical overpotentials generated on the CE, while lateral conduction is carried mainly by the conducting substrate supporting the CE.

Ion motion takes place via diffusion of the electroactive species and migration considered here negligible on the addition of ionic support [33], while convection does not occur. The absence of convection is due to the porous nature of the electrode as well as the small electrode separation [34]. The ionic diffusion coefficients in the mesoporous layers are not affected and can be assumed identical to their bulk diffusion coefficient since the heterogeneity of the macro-homogeneous nanocrystalline film is of the nanometer scale [35]. The mean jump distance of the ions are more than an order of magnitude smaller than the pore dimension in a three-dimensional network of 20 nm particle packed superstructure [36]. Our recent study on ionic transport in mesoporous TiO_2 films [33] shows that the deviation of the diffusion coefficient of tri-iodide in the liquid filled pores from the free-stream value is negligibly small and therefore not influenced by a tortuosity factor. Diffusion coefficients in the liquid filled pores can not be considered necessarily unchanged in all three sections of the cell, an assumption dictated by the material structure, i.e. tortuosity and pore connectivity as well as the dimensions of the particle consisting the material. In addition, the double-layer can be considered a stagnant layer surrounding the nanocrystalline particles of similar thickness to the dye diameter, which includes of course the adsorbed sensitizer molecule, adding only to the particle size by less than 5% under the high ionic strength electrolyte conditions employed [33].

The overpotential η represents the sum of the mass-transfer (η_{mt}) and kinetic or charge-transfer overpotential (η_{ct}) overpotentials, which, on the basis of the equipotentiality axiom, applied here for the case of a highly conducting CE material, is independent of x. The intrinsic exchange current density of the CE material in the electrolyte at the initial concentrations, is denoted i_{o} (see Appendix in [32]).

6. Discussion

6.1. The solar cell characteristics

The system of equations describing the steady-state operation and defines the concentration profiles of iodide and tri-iodide (variation of concentrations with position along the x-axis inside the entire multilayer cell) as a function of the total current delivered. These concentration profiles formally correspond to the conditions fulfilled at the short-circuit position of the I–V characteristic of the PEC performance curve. Typical examples of experimental I–V curves are depicted and the shown behavior analyzed in Section 6.4 of this discussion. In the subsequent analysis of the experimental results the following notions are necessary in order to evaluate solar cell performance: the short circuit current (I_{sc}), defined as the cell current under illumination at zero cell voltage bias, and the open circuit voltage (V_{oc}) referring to the voltage bias value that corresponds to zero overall cell current. The power output of the cell is maximized ($W_{\max}$) at the peak power point of the I–V characteristic, and $W_{\max}$ and the fill-factor (ff) are mutually defined as a function of the short circuit current (I_{sc}) and the open circuit voltage (V_{oc}) via the expression: $W_{\max} = \mathrm{ff} I_{\mathrm{sc}} V_{\mathrm{oc}}$. The overall energy conversion efficiency of the solar cell can also be defined as $\eta_{\mathrm{eff}} = 100\, W_{\max}/W$ (%), where W the incident irradiation intensity in $\mathrm{mW/cm^2}$.

6.2. The counter-electrode properties

In view of the use of organic electrolytes of variable viscosities and room temperature molten salts in nanocrystalline solar energy conversion systems there has been an imminent need to minimize the energy losses around the maximum power point (due to a low fill-factor) as well as the performance limitations imposed on the system by iodine reduction, thus, posing much higher demands on the electrocatalytic properties of the CE. As most electrode materials exhibit slow intrinsic kinetics for tri-iodide reduction with a rare exception the Pt cluster catalyst [37], other ways for producing higher performance CEs are sought.

With the aid of the developed model it is desirable to assess alternative possibilities for CEs in nanocrystalline solar cell design. For a given CE length, a, higher exchange currents can be achieved through surface area (porosity or specific surface), with an effective exchange current:

$$i_{\mathrm{o,eff}} = i_{\mathrm{o}}\,(\mathrm{surface/volume})\,a$$

The notion is expressed above that an excessively high kinetic overpotential on a CE can be compensated by increasing the effective surface area, thus increasing the effective exchange current density.

An example of various porous material constructions and their kinetic performance is summarized in Table 2, using methyl-ethyl-morpholinium iodide: 0.45 M, I_2: 50 mM, in n-methyl oxazolidone as solvent. From the experimental estimation of the effective exchange current values, it appears feasible to increase by orders of magnitude the activity of an electrode towards tri-iodide reduction. By comparison of these values one can easily conclude that the carbons and the Ru oxides seem to display increased activity as their exposed surface area is enhanced.

On the other hand, another aim of the porous CE would be to form a better conducting electrode to replace the conducting glass current collector, which electrode should, therefore, combine high tri-iodide reduction kinetics with lateral conduction.

One could design a CE to the kinetic specifications required for optimum performance from the point of view of tri-iodide reduction overpotential when assuming the possibility of ‘colloidal’ or porous film fabrication. For example, an electrode comprised of colloidal particles with diameter $d = 25\,\mathrm{nm}$ and ‘sintered’ into a film of porosity $\varepsilon_{\mathrm{ce}} = 0.5$ and thickness $a = 10\,\mu\mathrm{m}$, would have a specific surface of $\mathrm{A} = 6\,(1-\varepsilon_{\mathrm{ce}})/d = 1.2 \times 10^8\,\mathrm{m^{-1}}$ (randomly packed sphere model) and therefore an effective exchange current density $i_{\mathrm{o,eff}} = 120\,\mathrm{mA/cm^2}$, given an ‘intrinsic’ exchange current of $i_{\mathrm{o}} = 0.1\,\mathrm{mA/cm^2}$ for the smooth material. In other words, the charge-transfer resistance $R_{\mathrm{ct}} = 1/(2\,f\,i_{\mathrm{o}}) = 128\,\Omega\,\mathrm{cm^2}$ reduces to $R_{\mathrm{ct,eff}} = 1/(2\,f\,i_{\mathrm{o,eff}}) = 0.107$, merely by the surface effect. At this point one should address the fundamental question whether increasing the kinetic performance of the CE in such a manner would result in mass-transfer

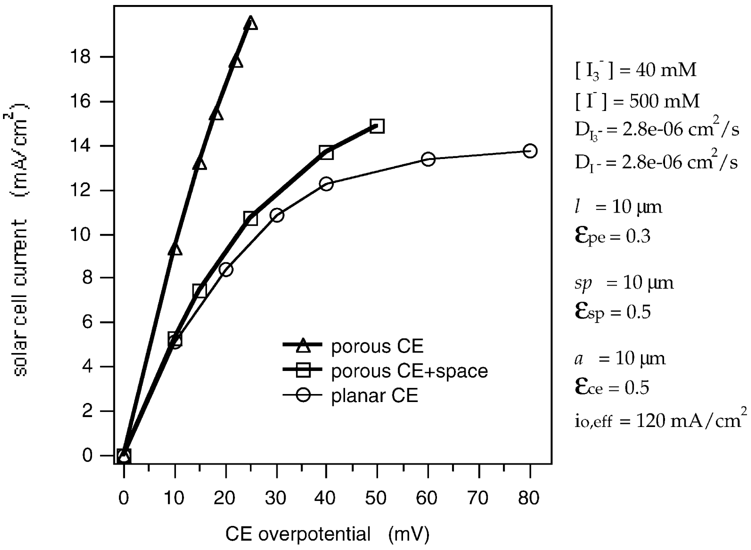

Fig. 6. Model prediction of cell current density vs. total CE overpotential for three different selections of cell configuration and under the corresponding layer parameter conditions shown. The photoelectrode model calculation assumes a colloid diameter of 25 nm and a dye diameter of 1.2 nm, defining a sensitizer concentration of 193 mM. The extinction coefficient ε_{540}, of the dye at $\lambda = 540$ nm is 12.5 mM^{-1} cm^{-1}.

limitations, and how they would manifest in terms of cell performance.

6.3. Numerical mass-transfer model results

The numerical solution of the system of equations with boundary conditions [32], was performed by a program on the application software MATHEMATICA®, based on LSODE that is characterized by the automatic switching between a non-stiff Adams method and a stiff Gear method [38]. The influence of substituting the planar CE for the porous one is illustrated with the aid of Fig. 6, depicting the comparison of calculated data from the numerical solutions of the system of differential equations produced for the particular set of conditions and parameter values shown. The decrease in the overpotential required to operate a 10 µm porous CE, is noteworthy. In fact, efficient solar cells cannot operate above 10 mA/cm^2 with a planar CE, whereas a typical porous CEs is still operating comfortably at double that current. The effect of adding an intermediate separator of 10 µm as insulator or scattering layer to the previously described configuration appears to have an important effect in reducing the limiting current for the same conditions of operation. The maximum current density attainable is that for which, the reduction of I_3^- occurs as fast as it can be supplied by diffusion to the cathode plane. Its concentration in the vicinity of the cathode is then zero for the limiting current density. Close to the limiting current, the CE can generate considerably high mass-transfer overpotential values. Total depletion of tri-iodide is virtually impossible in the porous CE case, as local current density adjusts to concentrations within the porous CE, in a self-regulating manner. For the planar CE it is assumed that a large excess of I^- is present and that the diffusion of I_3^- towards the cathode should at some point become limiting. Typical results from the model, in form of concentration profiles, can be seen in Fig. 7, when converging at a CE overpotential of $\eta = 50$ mV under the conditions and parameters specified in Fig. 6.

The current density in the CE region, seen in Fig. 8, varies greatly as mass-transfer controls differently the kinetic component of the overpotential from one end to the other. An apparently inefficient utilization of the CE material can be observed in this case. A relatively small percentage of the CE mass is contributing to the total current flowing through the cell. However, it appears that the supply of tri-iodide from the excess electrolyte contained within the pores of the whole CE play a significant role in reducing the mass-transfer overpotential build-up.

Given that the sum of the mass-transfer and kinetic overpotentials must assume a constant value under the steady-state, the former should be higher in value toward the right side of the CE than the left, where the local

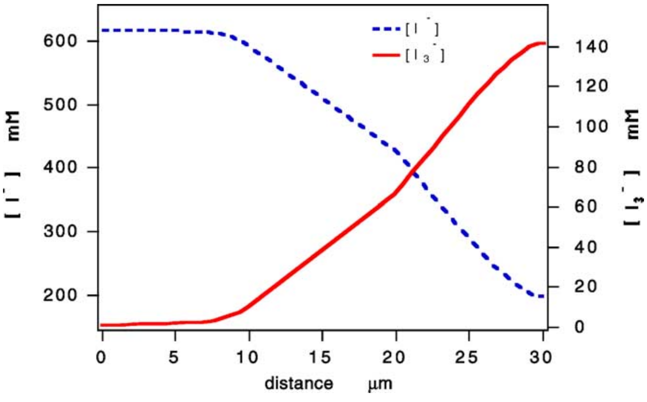

Fig. 7. Concentration profiles in the multilayer cell configuration generated for the parameters shown in Fig. 6. The current flowing through the system is 14.9 mA/cm^2 at a CE overpotential of 50 mV.

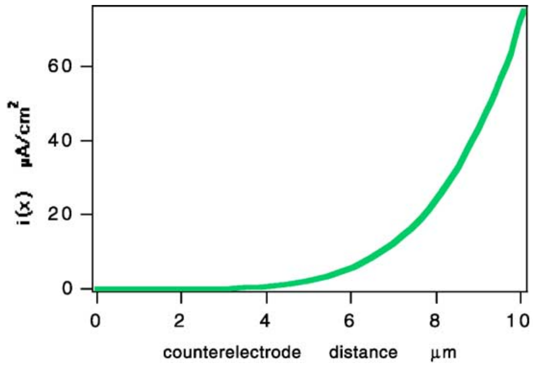

Fig. 8. The local current density in the CE layer under the operation conditions depicted in Fig. 7.

current produced severely diminishes together with the charge-transfer (kinetic) overpotential. Fig. 9 exemplifies this fact along with depicting the electrolyte redox potential shift throughout the other domains of the cell due to the variations in the electrochemical couple concentrations in the other layers of the cell as well. At the far end of the photoelectrode a positive shift in potential of 50 mV is registered, producing more undesirable ‘dark current’ (reaction VII) corresponding to this potential increase, a situation that would not influence the performance characteristic curve close to the short circuit but the current as we approach the $I-V$ maximum power point.

The above described situation is a result of the excessive accumulation of tri-iodide and the even stronger depletion of iodide in the vicinity of the photoelectrode, with a porous three-dimensional CE or/and the presence of the spacer layer. This behavior is quantified in the model results of Fig. 10, taking the concentrations of both redox species at the outer right edge of the photoelectrode as a function of current delivered by the cell, for the three different cell configurations examined. It should be noted that a similar trend has been analyzed in the simpler case of a planar CE-photoelectrode configuration with either the two separated by a layer of bulk electrolyte [32] or with the electrodes unseparated but having the bulk layer added on the side of the CE.

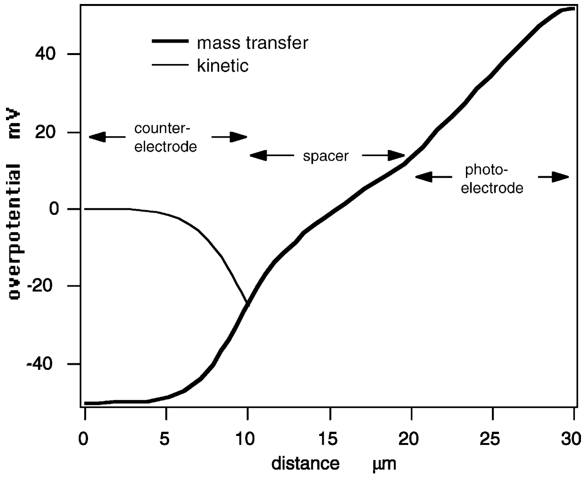

Fig. 9. The concentration overpotential throughout the whole cell and in the CE region; the charge transfer overpotential (thin line) under the conditions set in Fig. 9.

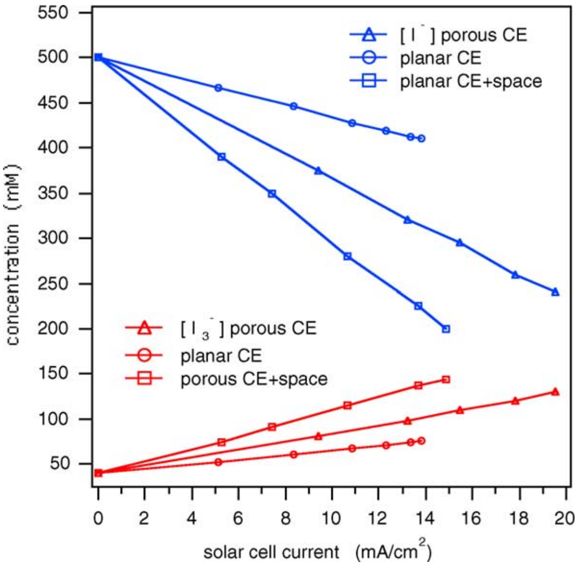

Fig. 10. Concentrations of iodide and tri-iodide at the far right side of the photoelectrode as a function of current density passing through the cell, for the three different cell configurations. All parameters and conditions are the same as in Fig. 6.

Iodide depletion on the photoelectrode side of the cell results in a decrease in injection efficiency through the decrease of the sensitizer regeneration rate, given the dependence of the kinetics of this reaction on the iodide concentration. In practical devices, the I^- concentration used, is always much larger than the $I_3{}^-$ concentration. However, for the sake of completeness, we must state here that if the I^- concentration selected was small enough, then mass transport of I^- towards the right might become limiting, inasmuch as, at steady state, there would not be enough I^- to ensure the reduction of the oxidized dye occurs on the right hand side of the cell in order to prevent the recombination reaction from taking place to a significant extent, and allow for a successful injection due to efficient sensitizer regeneration. This iodide threshold has been experimentally determined and for the solvent viscosities pertinent to our conditions here, is around 0.5 M [39,42]. It can be seen that the multilayer cell configurations are prone to photoelectrode injection limitations as efficiency is negatively influenced by iodide depletion at the photoelectrode. On the contrary, CE operation is at the same time facilitated by much less tri-iodide depletion and by the positive influence on the local exchange current density of both redox concentrations maintained at a reasonably high and stable level. This results in the CE operating at a much lower overpotential for the same cell current.

The above results have considered the diffusion coefficients unchanged in the different layers of the cell. The decrease of their value in poorly structured materials (large two-dimensional particles and porous layer structures with high tortuosity) creates greater extremes in the concentrations, with understandable consequences, as can be seen in the following section.

Another aspect of detriment to the injection efficiency of the solar cell incorporating a porous layer CE is the photon absorption loss due to tri-iodide in the spectral region below 500 nm. The optical density of tri-iodide, with $\varepsilon'_{380} \cong 19.4\,\text{mM}^{-1}\,\text{cm}^{-1}$ at 380 nm ($\varepsilon_{380} \cong 9.2\,\text{mM}^{-1}\,\text{cm}^{-1}$ for the dye [19]), at the concentrations for the porous layer examples evaluated above is high enough to absorb up to 30% of the radiation intensity at 380 nm, and the above figure will increase with the initial tri-iodide concentration, photoelectrode porosity and layer thicknesses, and with decreasing diffusion coefficients.

6.4. Supporting experimental evidence

A monolithic solar cell design has been developed by Kay and Grätzel [40], comprising a full carbon CE of 50–70 μm, and a 10–20 μm light diffusing/reflecting layer comprised of 300 nm colloidal rutile TiO_2 particles mixed with 10% ZrO_2 20 nm particles as binder and insulator. The porosities of these layers were estimated at around 50%. The CE mixture of 20% soot and 80% graphite has very good lateral conductivity matching that of CTO glass (sheet resistance 5–10 Ω) for the above thickness and significantly improved catalytic activity towards tri-iodide reduction (see Table 2). Acetonitrile based electrolytes were used for this type of cell, expecting the charge-transfer resistance of the CE to be so low that reduction kinetics would influence to a negligible extent the solar conversion characteristics of the cell at maximum irradiation (1 sun AM1.5). It was observed that this cell configuration began to manifest severe performance losses from illumination power levels of 0.5 sun and higher, due to lower photocurrent values even when using a low viscosity acetonitrile electrolyte.

From the materials point of view, the graphite powder particles comprising the CE have larger than desirable the two of its dimensions (approximately 10 μm), unlike a more favorable case with, e.g. carbon nanotubes where only one of the dimensions is of the micrometer scale [41], allowing the description plate-like crystals or flakes instead of colloidal particles, that tend to be aligned flat in the lateral plane as shown in Fig. 11. This structure improves lateral conductivity but results in an important depression in the ionic diffusivity in the normal direction within the CE domain. The effect was calculated with the model by assuming a redox species diffusivity in the counterelctrode domain of half of that in the others, which is for acetonitrile 4×10^{-6} and $8 \times 10^{-6}\,\text{cm}^2/\text{s}$, respectively, in a cell with a 60 μm CE, a 20 μm separator and a 10 μm photoelectrode. It is apparent from the model simulation of an approximation to the above described conditions (Fig. 12), that the limitation is not as much tri-iodide as iodide induced. It is observed that even with the choice of the very low viscosity solvent acetonitrile, the iodide profile dips into low concentrations within the photoelectrode region, conditions decreasing photoelectron injection efficiency as the electrode is iodide starved. Conversely, tri-iodide accumulation is occurring to a considerable extent, creating losses related to dark current and spectral photon absorption. One can see from the tri-iodide profile that it is still far from depleted within the CE region and particularly near the spacer, hence forcing the necessary

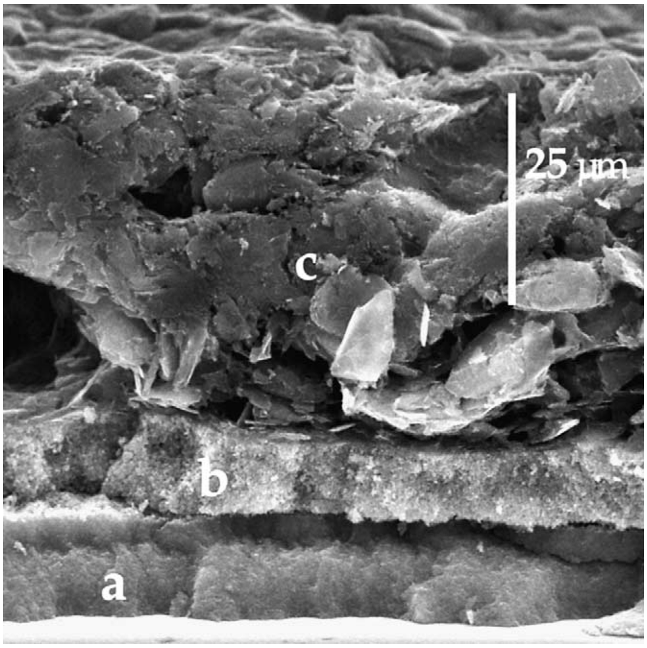

Fig. 11. SEM cross-section (fracture) of the multilayer photoelectrochemical solar cell described. Distinguishable are the principle three layers of the device: (a) anatase TiC_2 nanocrystalline film photoelectrode, ~10 μm, (b) the light diffusing insulator layer, 10–20 μm and (c) the 60 μm porous carbon CE comprised primarily of flat graphite particles.

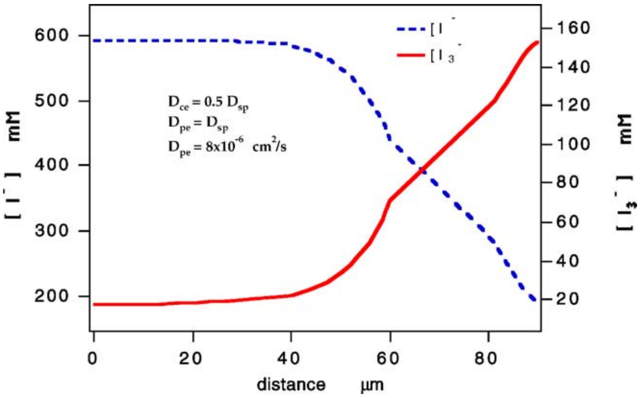

Fig. 12. The calculated concentration profiles for an actual multilayer cell construction comprising a 60 μm porous graphite layer, a 20 μm rutile TiC_2 scattering layer, and a 10 μm photoelectrode, and dimethyl-propyl-imidazolium iodide 0.5 M and 40 mM tri-iodide, at operating current $18\,\text{mA/cm}^2$ and CE overpotential 18.3 mV; all other parameters identical to Fig. 7.

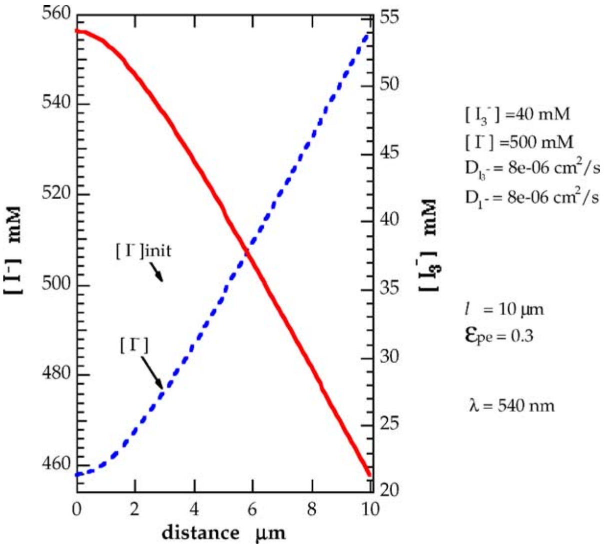

Fig. 13. The calculated concentration profiles for a planar CE construction, at operating current 18.3 mA/cm^2 and all other parameters identical to Fig. 12. The total CE overpotential is in this cell 14 mV (12 mV due to mass-transfer).

concentration gradient to be built up from increased levels on the photoelectrode side. A similar semi-empirical interpretation could be adopted to rationalize the form of the iodide profile, since the iodide concentration near the spacer is not ’permitted’ to reach higher values, the profile is forced to plunge into lower values in order to establish the required iodide flux. The implications of this configuration are intensified when the D_{sp} in the spacer layer is decreased due to the large size of the particles or of formed aggregates, stemming from the very nature of the medium as an efficient diffuse reflector.

It is easier to understand the effect of the multilayer cell design by comparison to the planar CE cell configuration without spacer, at the same cell current density and tri-iodide reduction effective activity, i.e. CE exchange current, as shown in Fig. 13. It is observed that within the photoelectrode film the redox concentration modulate around the initial electrolyte levels, hence avoiding extremely high or low values, maintaining dark current to a minimum and keeping the iodide within ‘safe’ range, for the photoelectrode dye regeneration function.

Last, an interesting design could use a low cost (compared to CTO) and very low porosity conducting (graphite) sheet (∼50–100 μm), with an inner interfacial layer of catalyst; this combines conductivity with facile CE kinetics as well as tri-iodide mass-transfer compensation at steady state, that is to say, reduced concentration polarization that has a bearing on the fill-factor.

A clear effect of the cell configuration on the short circuit current is demonstrated in the following comparisons, the experimental instrumentation and procedures have been described elsewhere [20]. Using the solvent glutarodinitrile (5.8 mPa s) and the salt dimethyl-propyl-imidazolium iodide at 0.5 M and 50 mM tri-iodide, a planar electrode cell delivered reproducibly over many trials a current 11–12.5 mA/cm^2 and had a 0.65 fill-factor at 1 sun. The same photoelectrode coupled with the carbon porous CE

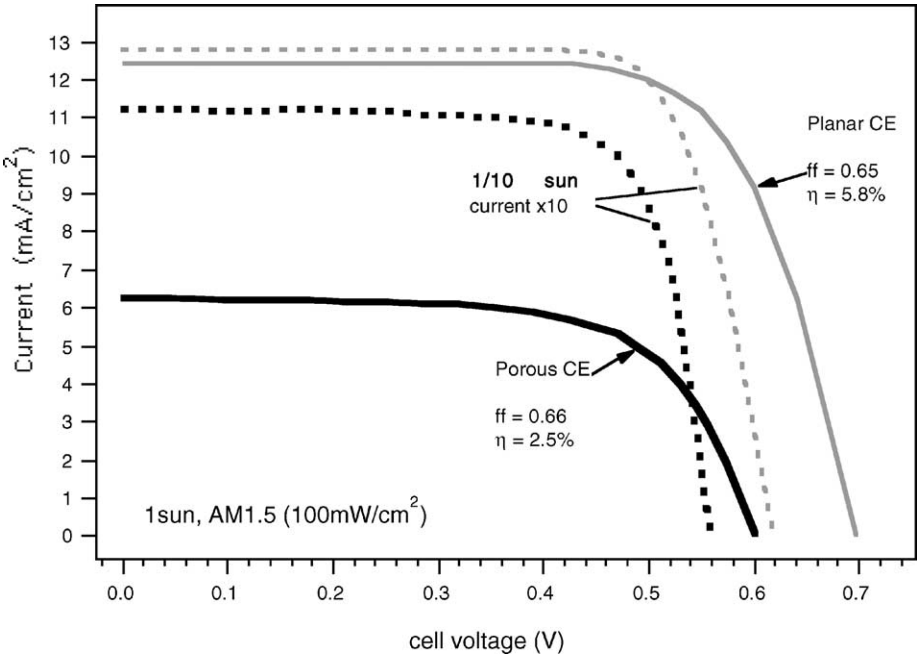

Fig. 14. The experimental current–voltage characteristic performance curves for the three layer photoelectrochemical solar cell displayed in Fig. 11, and for the standard single layer-planar CE cell, incorporating identical photoelectrodes and subjected to the same experimental illumination of 1 sun (AMI.5) and 1/10 sun conditions, as well as utilizing the same electrolyte. The electrolyte contained 0.5 M dimethyl-propyl-imidazolium iodide (DMPIml) and 50 mM tri-iodide in the solvent glutarodinitrile.

delivered 6.1 mA/cm^2, the fill-factor being the same (ff = 0.66) under identical conditions (see Fig. 14), resulting in a peak power efficiency reduction to half that of the planar CE cell. Moreover, at 0.1 sun illumination both solvents gave the correctly expected linear to the light intensity I_{sc} response [19,20]. The fact that the I–V characteristics in all cases exhibit the extended flat-constant-value region at the I_{sc} eliminates tri-iodide limitation as the cause (see also Fig. 6) of the non-linearity of I_{sc} with respect to irradition intensity. Indeed, tri-iodide limitation at the CE manifests as an increase in the mass-transfer overpotential and therefore a decrease in the fill-factor as a result of increased slope and curvature in the V_{oc} region [20,32]. Clearly, it is the influence of local iodide concentration in the vicinity in the photoelectrode domain that is limiting overall cell performance, as iodide is severly depleted, indicated by the model, and most dramatically at light incidence side of the photoelectrode where the largest portion of the photon flux is absorbed and therefore sensitizer regeneration efficiency has the greatest effect on the overall current/efficiency of the cell. These experiments demonstrate that the electron injection efficiency of the cell depends on electrolyte viscosity at elevated light intensity (1 sun). This conclusion is also substantiated by the fact that experimental fill-factors on the I–V characteristic curves are not reduced as a consequence of changes in the CE configuration. It is noteworthy that changing the solvent to AcN brought the current to above 11 mA/cm^2 in the planar as well as for the porous CE cell, when keeping unchanged the redox concentrations and species in the electrolyte. In this very low viscosity solvent (0.35 mPa s), I_{sc} are approximately linear to the irradiation intensity in the range examined, i.e. 1 sun (100 mW/cm^2) illumination.

7. Conclusions

For the study toward an alternative CE design and a complete multilayer solar cell system, we have developed a mass-transfer simulation model that takes into account in more detail the geometric and structural properties of the multilayer solar cell configuration comprising a porous CE and a porous spacer layer.

The above analysis allows the concentration of the redox active species to be determined under steady state irradiation as a function of current density and location as well as determines the overpotential loss on the CE under operating conditions. The problem of transport and losses due to the variations in the redox concentrations within the different compartments of the cell permits the following conclusions to be drawn with respect to the main behavioral aspects of the system: (i) pronounced depletion of iodide in the photoelectrode region is caused in the situation where the total length of the cell is increased resulting in reduced injection efficiency of the device, (ii) tri-iodide ‘accumulation’ in the photoelectrode region occurs resulting in an undesirable increase in dark current (reducing the fill-factor) and photon absorption up to ∼500 nm (reducing current output), and (iii) a mesoporous CE decreases considerably the kinetic overpotential as well as decreases the mass-transport overpotential generated during solar cell operation, which can result in an effective extention of the useful current range when compared to a planar CE with the same effective exchange current and at a given initial tri-iodide concentration in the electrolyte.

In extracting benefit from alternative CE design it appears critical to be able to strike a healthy compromise between i_o, porosity, CE layer and spacer dimensions, depending on the PEC application power range and the properties of a given electrolyte. Possibilities certainly exist in low to medium power applications through attention to design details dictated from integrated cell models. Strategy towards achieving certain performance characteristics in multilayered PECs can be layed out and summarized with respect to: (a) structural improvement of porous CEs, i.e. decrease porosity with concomitant increase in specific surface area; decrease in reflecting/scattering spacer layer thickness and porosity increase; fabrication of CEs from particles of colloidal dimensions in order to attain higher diffusion coefficient values, (b) CE material properties improvement, i.e. increase i_o (by low amounts of catalyst deposition, e.g. catalytic Pt cluster); to increase conductivity with ultimate aim a thinner CE; choice of materials that would have the ability to sinter or bond thus delivering mechanical strength and conductivity combined with a mesoporous structure of high pore connectivity.

7.1. Part III. The mediator electrolyte junction

7.1.1. Performance of organic solvent/molten salt electrolyte systems

Several organic electrolytes and their combination with room temperature molten salts systems have been used to scrutinize the performance characteristics, the stability and the mass-transfer effects in a photoelectrochemical regenerative device, as the latter is influenced and can even be limited by the local concentration and mass-transport of the electroactive redox mediator species in the electrolyte phase. These molten salts appear to afford particular advantages over organic liquids as solvents for solar cell electrolytes. Cell performance showed outstanding stability, with an estimated sensitizer turn-over in excess of 50 million. Hence, an investigation was carried out on the physical–electrochemical properties of MHImI and its mixtures with organic solvents such as *n*-methyl-oxazolidinone, acetonitrile and with other lower viscosity molten salts such as methyl-butyl-imidazolium triflate. The repercussions of these properties on solar cells is described experimentally by the performance of practical application devices. Simulation models of the mass-transport in the nanocrystalline solar cell help illustrate operational aspects such as concentration profiles, the limiting currents, the anticipated mass-transfer overpotential as a function of current density, and to make projections into how the properties of molten salt electrolytes can be better exploited toward this practical end.

At this present stage of cell development, an electrolyte based on salts dissolved in organic solvents is most commonly used. Such an electrolyte presents certain drawbacks: (a) The volatility of the solvent implies that the construction of the cell must be absolutely tight. (b) The solubility of the salts could be overstepped when the cell works at lower temperature than anticipated, resulting in precipitation. (c) Solvents are often incompatible with the glues used to seal the cell. In order to avoid one or all of these problems, other kinds of electrolyte should be sought. One possibility is to use an ion conductive solid but in the case of solid junction, the quality of the interface is critical. This is one of the reasons why electrolytes based on polymers where developed. The ability of the polyelectrolytes, polymer or gel electrolytes to form films and the elasticity of the latter allow good interfaces to be obtain, at a quasi-solid state. In the case of a porous electrode, the broader category of polyelectrolytes may not be as convenient, since the filling of the pores requires more technical attention, however there would certainly be advantages in terms of stability. Hence the reported choice of electrolytes based on room temperature molten salts, which combine advantages of solvent based electrolytes and that of polyelectrolytes. It will become apparent in the following sections that the major challenge with such electrolytes is to not confine them to moderate power applications due to the higher viscosities of these salts. The molten salts can play the role of the solvent only [43], or be involved in the mediator electrochemical processes. A mixture of an electroactive molten salt with an electroinactive one being less viscous seems to be the right compromise. Much research has been done in our group to identify room temperature molten salts with very low viscosities and other suitable properties [44].

Molten salts are ionic liquids and as such can be utilized in a wide range of electrochemical applications where high conductivity and ionic mobility are required. Their ionic nature renders them negligibly volatile in the liquid state. These properties as well as relatively low viscosity, the large electrochemical window, thermal stability, miscibility with solvents or other salts and hydrophobicity are a few of the desirable qualities found in certain molten salts synthesized in our group and reported by others [44,45], making them attractive for use as electrolytes and solvents in the dye-sensitized nanocrystalline solar cell. The methyl-hexyl-imidazolium iodide (MHImI) has been found, thus far, to be the least viscous iodide molten at room temperature, not sensitive to water and stable under the operational conditions of the dye-sensitized nanocrystalline TiO_2 photoelectrochemical cell utilizing the iodide/tri-iodide couple as redox mediator, and will thus constitute the basis for the analysis in the following sections. As would be by now apparent, during the mediator regenerative cycle, the total voltage consumed in order to maintain the CE function is the sum of the kinetic and the concentration polarization overpotentials, the latter being dependent on the mass-transport of iodide/tri-iodide within the cell. The deviations in the local concentrations of iodide and iodine from their initial open circuit values develop this additional potential loss. In the nanocrystalline photoelectrochemical cell, the cathodic reaction (reduction) is always confined to the planar surface of the CE, whereas the electro-oxidation takes place on the surface of the nanoporous semiconductor in contact with the anode current collector of the solar cell; tri-iodide is depleted at the cathode and iodide depleted at the photoanode. The mass-transfer of iodide is of consequence, as a lower threshold for iodide concentration must be observed in order to efficiently intercept the oxidized state of the sensitizer. On the other hand, tri-iodide depletion at the CE will affect cathode performance, and can even limit the operation of the solar cell.

Consider a thin-layer device mimicking in a simplified fashion the operation of the solar cell. This thin-layer cell would be comprised of a planar anode and cathode and at steady-state the concentration overpotential at the cathode, $\eta_{\mathrm{mt},c}$ is given by the following relation when the species O is limiting (see Appendix [20]):

$$\eta_{\mathrm{mt},c} = E - E_{\mathrm{equil}} = \frac{RT}{nF}\ln\left(\frac{C_{\mathrm{O}}(x=l)}{C_{\mathrm{R}}^{3}(x=l)}\Big/\frac{C_{\mathrm{O}}^{*}}{C_{\mathrm{R}}^{*3}}\right) = \frac{RT}{nF}\ln\left(\frac{(1-y)(\omega\mu)^{3}}{(\omega\mu+3y)^{3}}\right)$$

where $\mu = D_{\mathrm{R}}/D_{\mathrm{O}}$, $\omega = C_{\mathrm{R}}/C_{\mathrm{O}}$, $y = I/I_{\mathrm{lim},c}$, $C_{\mathrm{O}}^{*}, C_{\mathrm{R}}^{*}$ initial concentrations.

Therefore, the mass-transfer overpotential in the thin-layer cell depends, from this first approximation, on the limiting current value, which in turn can be optimized by maximization of the diffusion coefficients. In following work the diffusion coefficients were determined by limiting current measurements [46], tri-iodide being the current limiting species, in the cell. At the limiting current, I_{lim}, the one-dimensional linear diffusion law produces a linear concentration profile for tri-iodide under steady-state across the layer δ, which has the limiting value of zero on the cathode and $2C_{\mathrm{O}}^{*}$ on the anode. This allows the derivation of the relationship between I_{lim} and D_{O}:

$$I_{\mathrm{lim}} = 2nFC_{\mathrm{O}}^{*}D_{\mathrm{O}}/\delta, \quad D_{\mathrm{O}} = I_{\mathrm{lim}}\delta/2nFC_{\mathrm{O}}^{*}$$

where $n = 2$ considering the two electron reaction scheme. Thus, improved understanding of the mass-transfer behavior of iodide/tri-iodide in the generally more viscous molten salt electrolytes was one of the principle aims of this work.

8. Experimental

8.1. Chemicals and purification

The fundamental structure of these salts was according to the following formula:

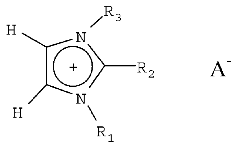

where A^- is the anion, e.g. I^-, Br^-, Cl^-, triflate (oTf^-), $N(CF_3SO_2)_2{}^-$ (Tf_2N^-), and R_1, R_3 alkyl substitutions ($C = 1$–7), and R_2 alkyl or H. The synthesis of all molten salts employed herein has been described elsewhere [44].

8.2. Instrumentation and techniques

The techniques were employed on symmetric thin-layer cells. The experimental set-up consisted of two platinized conducting glass electrodes held at constant separation by a mylar sheet between them. This two electrode arrangement was gradually polarized at a rate of 100 mV/s, until a current plateau was reached. Consequently, one electrode was exposed to anodic and the other to cathodic conditions. The limiting current resulting from the reduction of tri-iodide at the cathode could be thus measured. The above described technique was applied using electrolytes containing 40 mM I_2 dissolved in prepared mixtures of 1-hexyl-3-methyl-imidazolium iodide (MHImI), 1-butyl-3-methyl-imidazolium triflate (MBuImoTf) and NMO. The cell separation of 23 ± 0.3 μm and surface area of ca. 0.1 cm^2. All dynamic viscosity measurements were carried out on the Haake microviscosimeter-VT500 viscositester, thermally controlled by a Haake D8 thermostat–cryostat. Conductivity measurements were performed in a two platinum electrode conductivity cell (cell constant $K_{cell} = 0.68$, determined by aqueous KCl standard solution), under thermostated bath conditions. The ac impedance technique was employed and impedance measurements taken above 1 kHz [47], with estimated error less than 5%.

A thermally platinized cto glass was used as CE. The electrolyte was composed of 7 mM iodine in the MHImI molten salt, which synthesis has already been reported [44] The cell was assembled by holding together the working and the counter-electrodes and adding an electrolyte drop between these two plates.

Quasi-transparent solar cells were realized for low-power application, following the general process previously described for the fabrication of dye-sensitized, nanocrystalline solar cells [48,19]. The photoanode was made on ITO-coated glass yielding a 300 nm-thick nanoporous layer. The redox mediator solution was constituted of 10% hexyl-methyl-imidazolium iodide ($MHIm^+I^-$), 90% ethyl-methyl-imidazolium bis-triflylimide ($MEIm^+Tf_2N^-$) or triflate ($MEIm^+TfO^-$) and 5 mM iodine.

9. Discussion

9.1. Viscosities and conductivities of electrolytes

For unassociated liquid electrolytes, the empirical equation giving the temperature dependence of the dynamic viscosity is also applicable in ionic liquid systems [51]:

$$\eta = A\, e^{\varepsilon/RT}$$

where ε is the energy of activation for viscous flow.

Unless near the melting point where ions may associate into aggregates, the plot log η versus ($1/T$) can be reasonably fitted to a straight line in the narrow temperature window depicted in Fig. 15, although the behavior appears essentially non-Arrhenius, for the sake of obtaining an estimation of the activation energies. The experimental value for the activation energy ε for viscous flow is 6.1 kcal/mol for pure MHImI and follows a decreasing trend with MBuImoTf content in their mixtures, reaching 1.5 for the pure MBuImoTf. The experimental value for the activation energy ε, for e.g. the least viscous MEIm-bis-triflylamide is 0.17 kcal/mol. The empirical formula giving the viscosity of a mixture $\eta = \eta_1{}^{x1}\ \eta_2{}^{x2} \ldots \eta_n{}^{xn}$, where η_i, xi the viscosity and mole fraction of constituent i, respectively [49], appears to be generally applicable in the case of binary mixtures of molten salts and solvents. The accuracy of the formula is significantly improved by the way the mole fractions are calculated; whether the molten salts are taken as ionically dissociated or as molecules, as depicted in the example of Fig. 16. The prediction of the viscosity of multi component electrolytes is significant to the engineering of appropriate solvent systems for a particular solar cell

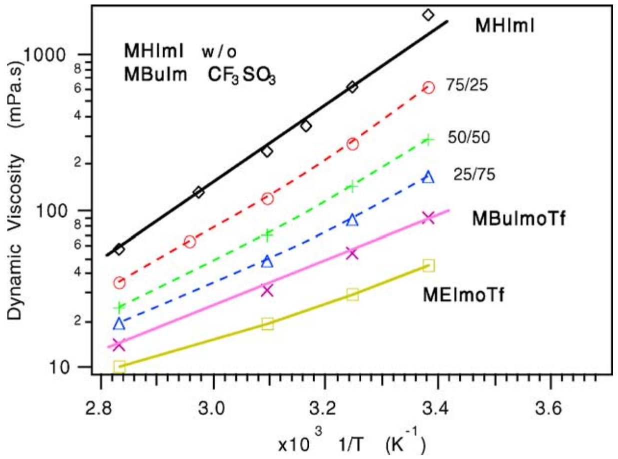

Fig. 15. Plot of dynamic viscosity (η) of some ambient temperature molten salts as function of reciprocal absolute temperature ($1/T$) and linear fit for MHImI data. Curves connecting experimental points are a guide to the eye.

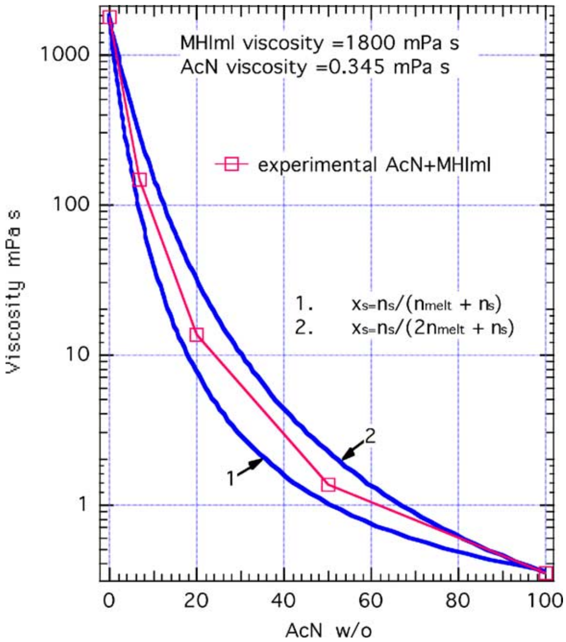

Fig. 16. Variation of molten salt MHImI mixture viscosity with weight percent content of co-solvent acetonitrile.

application, inasmuch as it can determine the operational mass-transfer limits of the electrolyte mediator. More exact correlations will be given in a following section. The measured conductivities of the much less viscous MEImoTf, as well as MBuImoTf and its mixtures with MHImI are shown in Fig. 17. It is worth noting that the specific conductivity dependence on temperature plots do not display Arrhenius behavior. Although it has been reported that MEImoTf does follow the Vogel–Tammann–Fulcher (VTF) type of equation [45], far-reaching conclusions were not warranted at this point of the study. The product of specific conductivity and viscosity is seen to measurably shift with varying temperature, the trend of which appears to depend on the system studied. In particular the pure neat molten salts decline with increasing temperature, whereas a system having a high content of NMO follows a strong increasing trend (Fig. 18).

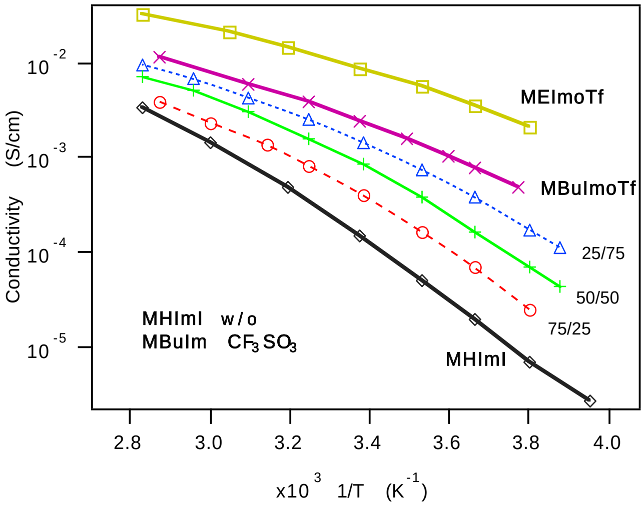

Fig. 17. Plot of specific conductivity (σ) of some ambient temperature molten salts as function of reciprocal absolute temperature (1/*T*). Curves connecting experimental points are a guide to the eye.

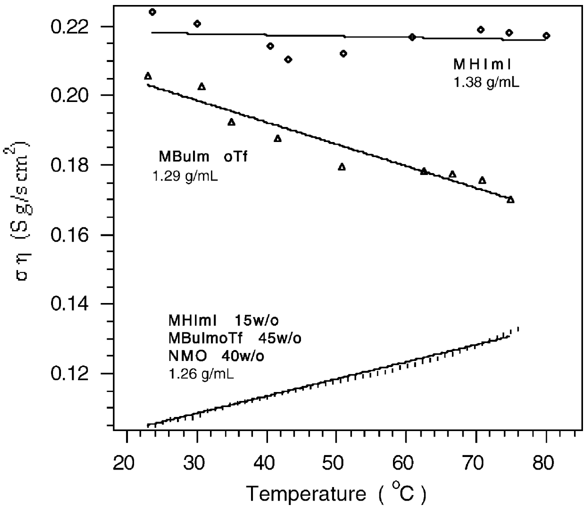

Fig. 18. Temperature variation of the product of conductivity and viscosity for different molten salt–solvent systems.

The conductivity of the 1:1-valent liquid salt can, to a reasonable approximation, be related to its viscosity (η), molecular weight (MW), density (d) and to the radii of their ions (r_a and r_c).

$\sigma = F\sum C'_i u_i = F(C'_a u_a + C'_c u_c)$, where C'_a, C'_c, u_a, u_c are the anion and cation concentrations and mobilities in the melt. It follows that $C'_a = C'_c = yC$, where $C = d/MW$ and $0 < y < 1$ the dissociation fraction. Therefore, $\sigma = yFC\,(u_a + u_c)$, the more accurate modified form of the Stokes–Einstein relation [50] correlates ionic transport to viscosity of the medium even in molten salts [51]:

$$D_a = \frac{RT}{6\pi N_A \zeta_a r_a \eta}, \qquad D_c = \frac{RT}{6\pi N_A \zeta_c r_c \eta}$$

where ζ_a, ζ_c are the anion, cation microviscosity factors. Combination with $D_a = u_a\,RT/F$, $D_c = u_c\,RT/F$, derives the relation between specific conductivity and anion, cation hydrodynamic radii.

$$\sigma\eta = yF^2 d/(6\pi N_A \mathrm{MW})[(\zeta_a r_a)^{-1} + (\zeta_c r_c)^{-1})]$$

which in principle is not a function of temperature. This equation includes the ‘correction’ factor ζ taking into account the specific interactions between the mobile ions in the melt.

The downward trend in the conductivity for the pure molten salts means that it is not catching up with viscosity drop of the pure molten salt. Neat molten salts are known to have positive thermal expansion coefficients [51], and the experimental trend with temperature is readily explicable in terms of the gradual decrease in density, as required by the formula, that is to say the slope reflects the change in molecular volume $V_m = \mathrm{MW}/d$ with temperature. The opposite trend observed in the NMO containing system can be explained by the dominant in this case role of the organic solvent in solvating the ion-paired portion of the molten salt, where the increase in the conductivity with temperature is higher than the lowering of its viscosity would dictate it to be. In the above case the $\sigma\eta$-temperature dependence should be a thermal competition between density d or molecular volume V_m and the microviscosities ζ_a, ζ_c, since $\zeta = 0.16 + 0.4\, r_i/r_L$, where r_L is the effective radius of the solvent molecule obtained from the molar volume and r_i the ion radius under consideration, r_L being temperature-dependent [50]. Another conclusion can be drawn from the comparison of $\sigma\eta$ for neat MHImI (4.7 M) and a dilute (0.5 M) in NMO. As follows from the above derivation:

$$\sigma\eta = y\, C\, F^2/(6\pi\, N_A)[(\zeta_a r_a)^{-1} + (\zeta_c r_c)^{-1})] \approx y$$

C constant can be justified for the same ions, and from which, by substitution of the measured σ, η as well as the nominal melt concentration, C, it appears that the dissociation fraction of the MHImI does not change significantly, at least not more than 10%.

9.2. Diffusion of iodine/tri-iodide in electrolyte systems

Limiting current experiments were conducted on the molten salt systems which contained a calculated amount of iodine. That the iodine is complexed to quantitatively form tri-iodide in the excess of I^- was verified by spectrophotometric characterization of given concentration of added iodine to MHImI, as evidenced by the tri-iodide absorption peaks at 292 and 363 nm [52]. The composition of the tested electrolytes ensures that tri-iodide is the current limiting species under the experimental conditions employed. Firstly because sufficient excess of I^- is provided, i.e. greater by 10 times the respective tri-iodide concentration, and secondly, of the fact that $D_{I^-}/D_{I_3^-} = 1 - 1.3$ from the reported literature in DMSO, DMF and AcN [53,54], adds in order to satisfy the condition $C_O D_O < 1/3\, C_R D_R$ [34], thus assuring a limitation by tri-iodide. The electrode separation and therefore the thin-layer thickness δ is 23 μm, and is equivalent to the Nernst diffusion layer of semi-infinite diffusion. It is well within the region $\delta < 200$ μm, where $I_{lim} \times \delta =$ constant [34], that is to say that the limiting current is linearly related to the electrode separation and therefore convection is negligible.

The high conductivity and ionic strength of the molten salt electrolyte minimizes the influence of the electric field, i.e. the migration of the electroactive and both charged iodide species. This appears particularly important for the case of tri-iodide, where the migration tends in the opposite of the desired diffusional flux toward the CE [32]. Tri-iodide migration under the electric field between the electrodes is in the direction from cathode to anode and therefore opposes the diffusion process. It thus follows that iodide migration adds to its diffusion in the cell. However, negligible ion migration of electroactive tri-iodide is expected under the above experimental conditions because of much higher iodide concentration and presence of non-electroactive cation as supporting electrolyte. For instance, in the case when molten salt is around 10%, the sum of iodide and the spectator ion concentration results in a close to 1% influence on the tri-iodide limiting current, and hence the diffusion coefficient determination [32].

Two MHImI containing systems were investigated, the one diluted with NMO, the other by the molten salt MBuImoTf as co-solvent, and comparison was made between them in terms of the mutual variation of viscosity and tri-iodide diffusion coefficient, namely the Einstein–Stokes ratio $D\eta/T$, or more commonly known at constant temperature as Walden product $D\eta$. All the above experimental values are concisely plotted as collective graphs in Fig. 19. As a general rule, the product of viscosity and diffusion

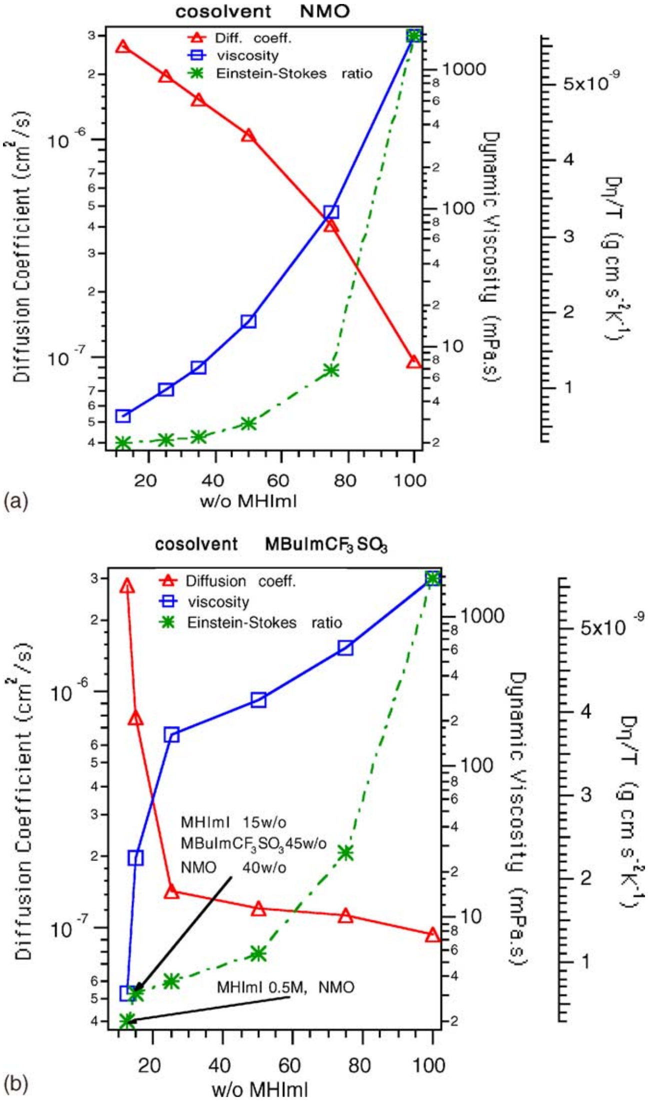

Fig. 19. Plot of tri-iodide diffusion coefficient, electrolyte dynamic viscosity and Einstein–Stokes ratio as a function of MHImI weight content in its mixtures with (a) NMO at 23 °C and (b) MBuImoTf at 25 °C, as co-solvents.

coefficient (Walden product) is approximately constant for a given solute in various solvents, at the same temperature [52]. In other terms, the product of viscosity and molar conductivity is approximately constant for the same ions in different solvents [55]. If the effective ion radius does not change in solutions with various viscosities and if association does not occur, Walden's rule is valid, i.e. $D\eta$ = constant or $\Lambda\eta$ = constant, where Λ is the equivalent conductivity. A varying rate of diffusion yields an excellent characteristic of individual states of aggregation among the component ions and the co-solvent molecules, ion pairing etc. However, the expectation with regard to Walden's rule that for very concentrated electrolytes ionic mobility would be additionally hindered as ion-pairing becomes influential, is opposite to the one indicated by the experiments in Fig. 19, where an increase in Walden product is observed with increasing iodide content of the binary system. The anticipated diffusion coefficient calculated on the basis of the Walden product in dilute organic solution is 16.5 times lower than the experimental value for tri-iodide diffusion in pure MHImI, and this not able to be attributed to the possible increase of the effective hydrodynamic radius of the diffusing moiety, as it is contradicted by the same phenomenon observed in the melt diluted MHImI. These results exemplify the change in the mechanism of mass or charge-transfer, suggesting a chemical (electron) exchange-Grotthus type charge carrier transfer mechanism influencing the overall transport, with increasing iodide concentration, which can be illustrated as follows:

$$I_3^- + I^- \rightarrow I^- - I_2 \ldots I^- \rightarrow I^- \ldots I_2 - I^- \rightarrow I^- + I_3^-$$

This is contrary to expectation that increased concentration induces more ion pairing, thus retarding the diffusion. The experimental curves show that tri-iodide diffusion does not obey the fundamental Stokes–Einstein equation $D = kT/6\pi r\eta$, as the Walden product defined as $D\eta$ is not constant at constant temperature, but is a function of electrolyte composition. Grotthus mechanism of charge transport is responsible for the fact that $D_{H_3O^+}$ in water is five times higher than expected from its dimensions, and D_{OH^-} much higher than predicted; analogously, $D_{H_3SO_4{}^+}$, $D_{HSO_4{}^-}$ in concentrated sulfuric acid is 50–100 times higher than for the other ions; and proton mobility in ice at 0 °C is 50 times larger than in water! [50]

The Einstein–Stokes ratio in dilute (0.5 M) solutions of iodide salts appears to have a small dependence on the organic solvent used, for e.g. PC, PC/EC 1:1, NMO, NMP, which is around 2.9×10^{-10} g cm s^{-2} K^{-1}, whereas the reported value in DMSO is 3.57×10^{-10}, in AcN 1.88×10^{-10} and in aqueous solutions 3.77×10^{-10} on the same scale [53,6,4]. It must be noted that the experimental Einstein–Stokes ratio remained constant at $(56 \pm 3) \times 10^{-10}$, practically invariable D and η, for varying tri-iodide concentrations in the pure MHImI salt, as shown in solutions containing 25, 50, 100 and 500 mM tri-iodide. However, a 4 M addition of iodine produced a dramatic drop in viscosity to 125 mP as from 1800, due to the dominance of the tri-iodide anion on the structure of the melt [56]. In order to compare the relative influence of the two co-solvents on the mass-transport of tri-iodide, the ratio of the Einstein–Stokes ratios for the two systems at different iodide contents was formed and tabulated in Table 3.

Table 3
Comparison of the Einstein–Stokes ratio deviation in the MBuImoTf and NMO diluted MHIml

MHIml w/o	Ratio of D_η/T(MBuImoTf/NMO)
100	1
75	1.92
50	2.20
25	2.50

The divergence in the $D\eta/T$ values between the two systems appears to indicate that NMO influences more by solvation or/and breaks down ion-pairing and consequently the chemical exchange between iodide/tri-iodide species to a greater extent than the purely ionic system does. However, if the mole-fractions of the solvents are calculated in the mixtures using the expressions that best fit the viscosity data (see Fig. 16), the variation of the Einstein–Stokes ratio as a function of solvent (or MHImI) mole-fraction is close to independent of co-solvent added.

9.3. Solar cell performance characteristics of neat MHImI and its mixture electrolytes

The experimental solar cell characteristic curves for pure MHImI molten salt electrolyte containing 7 mM iodine in Fig. 20 demonstrates how the pure melt is satisfactory and perfectly suited in situations where very low currents are delivered, that is at comparatively low light intensities (1 sun ≈ 120,000 lx). The short circuit current increases proportionally to incident light intensity (linearity). Linearity persists in this system until 100–150 μA/cm^2, under these conditions (depending mainly on film porosity and temperature), reaching finally its limiting value, as shown in Fig. 21. This

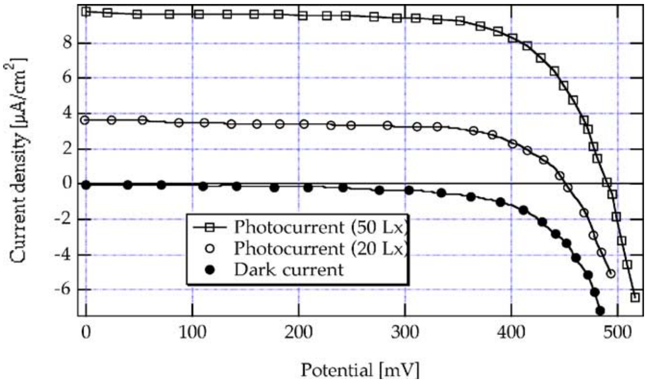

Fig. 20. Photocurrent and dark current vs. potential with indoor light. Incident power: 20 and 50 lx. Electrode surface: 0.6 cm^2. Equilibrium was reached before measurement of each point.

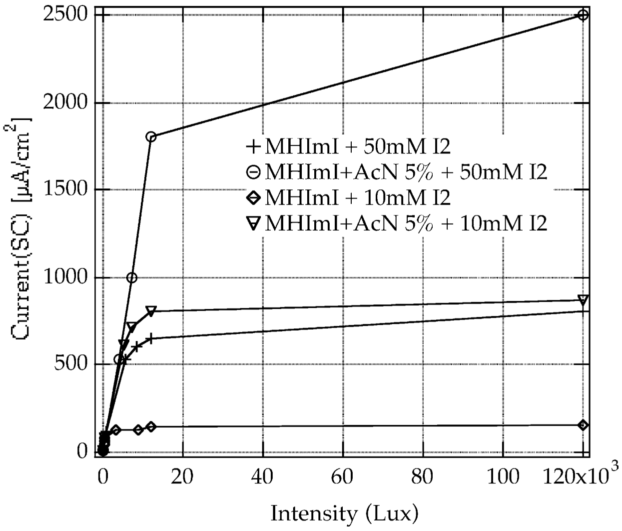

Fig. 21. Short circuit photocurrent with increasing incident light intensity for a 10 μm nanocrystalline solar cell, utilizing the MHIml electrolyte.

is a limitation imposed on overall cell performance solely due to the CE reduction reaction limit, as the iodide concentration is here extremely high, ca. 4.6 M, and would not be depleted. It is also obvious from Fig. 21 that the current limit depends strongly on the amount of tri-iodide in the electrolyte. Besides the addition of iodine, even the slightest decrease in electrolyte viscosity will increase the limiting current, as by addition of very little solvent, e.g. AcN. Linearity holds up to 1/10 sun in MHImI containing 50 mM iodine and 5 w/o AcN.

There are nevertheless restrictions on the amount of iodine added to solar cell electrolytes in order to complete the regenerative mediator operation. Tri-iodide absorbs strongly in the visible light range of the solar spectrum, with extinction coefficients in, e.g. propylene carbonate of 24,000 and 44,000 at 363 and 292 nm, respectively [52], as the tails of these absorption peaks extend well into the visible range. As a result, the increase of tri-iodide in the electrolyte will deprive the system of photons otherwise utilized for the generation of conduction band electrons, contributing to the net current output of the device. At the same time the issue of dark current becomes increasingly important with elevation of tri-iodide levels in the cell. The undesirable effects of the dark current are the result of enhanced rate of tri-iodide reduction on the photoanode, which kinetics are a function of tri-iodide concentration and become significant as the cell tends toward its maximum load on the characteristic, as the semiconductor Fermi level is shifted all the more negative. The dark current influences the open circuit voltage of the solar cell, and in more extreme cases the fill-factor of its characteristic (maximum power point). Within the context of the above detrimental effects, one aims at tri-iodide concentration minimization without compromising optimum performance on the CE.

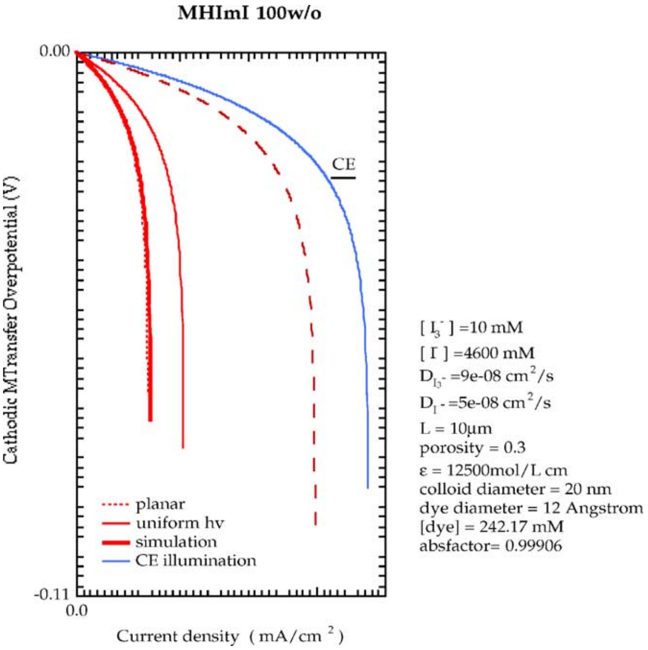

Fig. 22. The tri-iodide limiting currents in pure MHIml and 10 mM I_2, and the CE concentration polarization as a function of solar cell current according to the various illumination models describing solar cell operation.

Modelization of the inter-dependent electrochemical processes within the cell as an integrated system can provide insight into its functional limits in terms of mass-transport. By the simulation of the nanoporous PEC processes under, e.g. monochromatic illumination, given the diffusion coefficients of redox species, nanoporous layer porosity, colloidal particle diameter, sensitizer characteristics (extinction coefficient, molecule diameter), one can visualize the concentration profiles of both iodide and tri-iodide, estimate the required iodide levels in the electrolyte for a given application, and predict the mass-transfer overpotential and limiting current associated with tri-iodide reduction on the cathode, thus providing a measure of the performance limits with respect to iodide and tri-iodide functions in the solar cell, as a function of incident photon flux intensity or total current drawn. The implementation for the practical systems and certain implications of the simulation models will be discussed here, as the full derivation and comprehensive analysis is the subject matter of another publication [32]. Experiment has verified that the maximum current delivered by the nanocrystalline solar cell is in agreement with the predictions extracted from the models derived to describe the mass-transport of the electroactive species in the solar cell, as a function of illumination direction and light absorption mode. Although the experiment involves additional thermal effects and solar simulated light (variable extinction coefficient ε) the general applicability of the model is not impaired, and valid conclusions can be drawn [32].

Regarding the above low power application Fig. 22, for instance, shows the mass-transfer behavior of the CE within a solar cell, depending on the mode of light absorption: simulation corresponds to an ideal Beer–Lambert absorption law where $\text{flux}_{\text{abs}} = \text{flux}_{\text{inc}}\ (1 - 10^{-\varepsilon S x})$ and $S = 6\ (1 - \text{porosity})/(N_A\ d_{\text{col}}\ d_{\text{dye}}^2)$, the sensitizer concentration in the space of the cell [32]. The concentration polarization is a function of current delivered and varies for different modes of light absorption. In the same manner the limiting current on the CE is dependent on the mode of light absorption. It is, of course, desirable to extend the limiting current to higher values in order to achieve higher photocurrents when the photoelectrode is not limiting, and at the same time decrease the concentration polarization loss manifesting as the operational cell current increases from open circuit, in order to less effect the fill-factor.

In particular, the anticipated values for the limiting currents predicted from the model with illumination from the CE side have been experimentally proven to be correct. Although four times higher currents have been measured by CE illumination at 1 sun, there are experiments that give somewhat less, because of the slightly impaired photoelectrode efficiency, due to a higher rate of conduction band electron recombination the thicker the films [57], and in other cases resulting from a red shifted light source spectrum.

Iodide concentration has an effect on the mass-transfer overpotential, but naturally not on limiting current. To exemplify this, the concentration polarization at, e.g. 40 μA/cm^2 for the photoelectrode illuminated-simulation model for the case of pure MHImI (ca. 4600 mM iodide) is just below 6 mV, whereas the corresponding value in an assumed 100 mM in iodide and all other parameters identical, increases to 10 mV merely as a result of variation of iodide concentration alone.

Experiment has revealed that solar cell electrolytes containing above 20 w/o MHImI in solvents such as NMO or Glutaronitrile, display an improvement in solar cell linearity and have increased fill-factors at 1 sun. Linearity is affected, besides the inefficient tri-iodide transport, by the local depletion of iodide in the vicinity of the oxidized dye, resulting in recombination rather than electron injection into the semiconductor. Obviously a higher concentration of iodide in the electrolyte provides for efficient dye interception even at high currents, when the concentration risks to reach its lowest threshold value. Iodide concentration threshold appears to be at about 0.3 M. That is to say that the requirement for efficient electron injection into the semiconductor is the subsequent S^+ interception, and that therefore iodide concentration should be always >300 mM in 3 mPa s solutions. PE illumination in solar cells containing around 0.4 M iodide (normally the level in low viscosity organic solvent electrolytes) and with a slightly higher viscosity can be easily depleted of iodide, especially close to the side of light incidence, where redox activity is far greater.

Fill-factor decrease is most often the result of the dramatically increasing concentration polarization at the CE with increasing current, especially when the tri-iodide limiting current is relatively low, i.e. low diffusion coefficient, low colloidal film porosity or even low initial tri-iodide concentration. It is conceivable that a high molten salt content, and

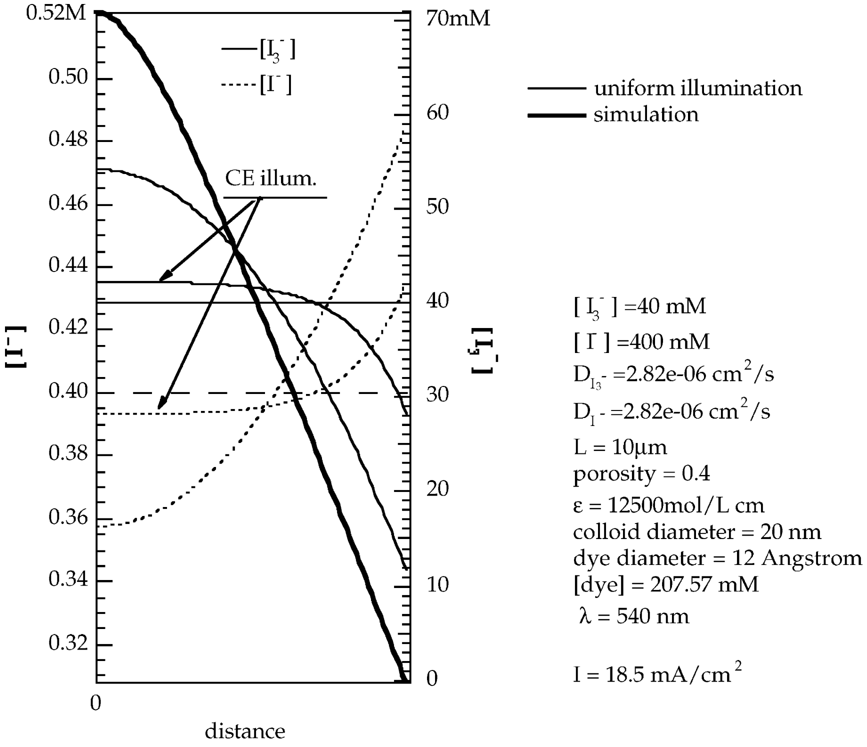

Fig. 23. Concentration profiles of iodide and tri-iodide in the nanocrystalline solar cell at steady state operation according to the various models describing the mode of illumination–light absorption.

Table 4
Photovoltaic characteristics of quasi-transparent, nanocrystalline, dye-sensitized solar cells operating with molten salts as electrolyte and redox mediator, measured under 0.020 AM1 illumination, aged under AM1

Illumination time (h) [a]	MEImoTf[b]			$MEImTf_2N$[b]		
	I_{sc}[c] (μA/cm^2)	U_{oc}[d] (mV)	ff[e] (%)	I_{sc}[c] (μA/cm^2)	U_{oc}[d] (mV)	ff[e] (%)
0	9.5	531	69	11.8	570	72
200	12.5	542	68	12.5	540	70
1000	13.0	535	68	11.3	510	69
1800	11.2	535	68	10.4	487	69
2400	9.8	527	68	9.0	491	70

[a] Suntest Original Hanau, AM1, with polycarbonate UV filter cutting at 400 nm. Cell temperature: 44 °C.
[b] Values given are means of three cells.
[c] Open-circuit voltage.
[d] Short-circuit current.
[e] Fill-factor.

therefore iodide, moderates the polarization fluctuations at the counter-electrode with current passed (Nernst equation), in addition to concurrently providing improved tri-iodide transport through the alternate mechanisms of chemical exchange-ion hopping.

Lower viscosity co-solvent addition into MHImI, even in small amount can affect important changes in the viscosity and consequently on the diffusion coefficients of the mediator. Onto this must be added the beneficial effect of the high iodide concentration with MHImI, which in itself, as has been shown, improves the mass-transport properties of tri-iodide. Measured diffusion coefficients of tri-iodide, fluctuate greatly with system composition: for example in acetonitrile: $>8.5 \times 10^{-6}$ cm^2/s, NMO: 2.8×10^{-6}, MHImI 10 w/o + $MEIm\text{-}NTf_2$: 3.4×10^{-7} and MHImI neat: 9×10^{-8}. However operation of a 10 μm solar cell at 18–20 mA/cm^2 with 40 mM tri-iodide and 0.3–0.4 porosity, requires around 2.8–3 $\times 10^{-6}$ cm^2/s for tri-iodide, in agreement to model (Fig. 23) and experiment alike (high power application). Acetonitrile diluted systems are promising as a relatively small weight percent content corresponds to significantly larger mole fractions and commensurate reductions in viscosity, with concomitant decrease in electrolyte vapour pressure. A projection for tri-iodide mass-transfer in a mixture of 25–30 w/o AcN in MHImI, corresponding to approximately 0.65 AcN mole fraction, an Einstein–Stokes ratio of around 6–7 $\times 10^{-10}$ g cm s^{-2} K^{-1}, and a maximum value 5–7 mPa s for the viscosity, determine a tri-iodide diffusion coefficient of 3.2 $\times 10^{-6}$ cm^2/s. This value, as indicated earlier, meets the requirements for operation at 1 sun, a fact which has been experimentally verified.

9.4. Low-power, quasi-transparent solar cells

The performance demanded in this case is low enough to not have to consider mass-transfer as a limiting factor. However, stability is of greater concern in such applications. After 200 days storage at 85 °C in the dark, the molten salt mixture had not altered the epoxy sealant. The cell performances stabilized after 80 days at 83% of the initial photocurrent and unchanged voltage. The cells display good stability towards illumination, as illustrated in Table 4 by the evolution of their photovoltaic characteristics. For all the measured cells, an initial current rise is observed, followed by a slow decrease to the initial value. The fluctuation of the photocurrent was found to be due to the temporary decrease in the tri-iodide concentration, as can be inferred by measurement of the diffusion limiting photocurrent under full AM1 irradiation. It is likely that this change in tri-iodide concentration arises from interference of the epoxy sealant. Adventitious contamination of the TiO_2 film may occur during the sealing with epoxy glue which is done prior to filling the cell with electrolyte. There is a risk of introducing liquid precured components of the epoxy into the porous TiO_2 structure. The better stability displayed by the cells containing the triflate-based molten salt is not yet fully understood, but the higher solubility of the epoxy glue in the hydrophobic $MEImTf_2N$ stands as the most probable reason.

In this particular case, over the 100 day AM1 illumination period, the short circuit current passing through the cell was about 0.6 mA/cm^2, implying an electron generation of 537 mol/m^2. Now, a cell absorption of 3% corresponds to a maximum sensitizer quantity of 11×10^{-6} mol/m^2. The sensitizer turn-over, defined as the ratio of electrons generated to the quantity of sensitizer, is therefore estimated at around 50 million electrons per dye molecule from these long-term tests. The low-power, however, non-transparent but low light intensity (up to 50 lx) sealed cells operating on pure MHImI melt with 7 mM I_2 as electrolyte display remarkable stability with time in the longer term after continuous exposure to 5000 lx at 50 °C.

10. Conclusion

Several organic electrolytes and their combination with room temperature molten salts systems have been used to scrutinize the performance characteristics, the stability and the mass-transfer effects in a photoelectrochemical regenerative device, as the latter is influenced and can even be limited by the local concentration and mass-transport of the electroactive redox mediator species in the electrolyte phase. These molten salt systems appear to afford particular advantages over pure organic liquids as solvents for solar cell electrolytes. Cell performance shows outstanding stability, with an estimated sensitizer turn-over in excess of 50 million. A range of physical and electrochemical properties present ambient temperature molten salts as practically viable, and therefore as attractive candidates for photoelectrochemical solar energy conversion devices. The high iodide concentrations possible with iodide molten salt systems; the enhanced iodine/tri-iodide transport as a result of either different solvation or the change in ion or charge transport mechanism; the formation of lower viscosity electrolytes with molten salts, e.g. MEImN$(CF_3SO_2)_2$ or organic co-solvents; the high ionic solubility and miscibility with other salts or organic solvents; the chemical and electrochemical stability; the higher boiling point or lower volatility; the optical transparency and the extremely low affinity to glues and resins used for PEC assembly, are some of the established qualities of these systems. The ionic transport of tri-iodide in the molten iodide appears to involve a different mechanism as compared to organic solvent-low iodide salt systems, which results in an at least 16-fold increase in the effective diffusion coefficient of tri-iodide in the pure molten iodide salt. Experimental solar cell performance conforms well to the limits predicted by the photoelectrochemical cell models which reveal an extended useful application range with molten salts as electrolytes.

References

[1] L.M. Dané, L.J.J. Jansen, J.G. Hoogland, Electrochim. Acta 13 (1968) 507.
[2] Yu.M. Povarov, I.E. Barbasheva, P.D. Lukotsev, Elektrokhimiya 3 (1970) 306.
[3] J.F. Coetzee, C.W. Gardner Jr., Anal. Chem. 54 (1982) 2530.
[4] V.A. Macagno, M.C. Giordano, A.J. Arvia, Electrochim. Acta 14 (1969) 335.
[5] S. Bhattacharya, K.K. Kundu, Bull. Chem. Soc. 68 (8) (1989) 2676.
[6] M.C. Giordano, J.C. Bazan, A.J. Arvia, Electrochim. Acta 11 (1966) 1553.
[7] K.J. Hanson, C.W. Tobias, J. Electrochem. Soc. 134 (9) (1987) 2204.
[8] K.J. Hanson, M.J. Matlosz, C.W. Tobias, J. Newman, J. Electrochem. Soc. 134 (1987) 2210.
[9] C.A. Koval, S.M. Drew, Inorg. Chem. 27 (1988) 4323.
[10] T. Bejerano, E. Gileadi, J. Electroanal. Chem. 82 (1977) 209.
[11] G.M. Berry, M.E. Bothwell, B.G. Bravo, G.J. Cali, J.E. Harris, T. Mebrahtu, S.L. Michelhaugh, J.F. Rodriguez, M.P. Soriaga, Langmuir 5 (1989) 707.
[12] A.T. Hubbard, R.A. Osteryoung, F.C. Anson, Anal. Chem. 38 (6) (1966) 692.
[13] J. Bruneaux, H. Cachet, M. Froment, J. Amblard, J. Belloni, M. Mostafavi, Electrochim. Acta 32 (10) (1987) 1533.
[14] J. Bruneaux, H. Cachet, M. Froment, J. Amblard, M. Mostafavi, J. Electroanal. Chem. 269 (1989) 375.
[15] S.I. Ho, K. Rajeshwar, J. Electrochem. Soc. 134 (3) (1987) 768.
[16] R. Tenne, M. Peisach, C.A. Rabe, C.A. Pineda, A. Wold, J. Electroanal. Chem. 269 (1989) 389.
[17] B. O'Regan, M. Graetzel, Nature 353 (1991) 737.
[18] M. Graetzel, Coord. Chem. Rev. 111 (1991) 167.
[19] M.K. Nazeeruddin, A. Kay, I. Rodicio, R. Humphry-Baker, E. Müller, P. Liska, N. Vlachopoulos, M. Grätzel, J. Am. Chem. Soc. 115 (1993) 6382.
[20] N. Papageorgiou, Y. Athanassov, M. Armand, P. Bonhôte, H. Pettersson, A. Azam, M. Grätzel, J. Electrochem. Soc. 143 (10) (1996) 3099.
[21] P. Bonhôte, A.P. Dias, N. Papageorgiou, K. Kalyanasundaram, M. Grätzel, Inorg. Chem. 35 (1996) 1168.
[22] J. Ross Macdonald (Ed.), Impedance Spectroscopy—Emphasizing Solid Materials and Systems, Wiley, New York, 1987, p. 20.
[23] M.T. Reetz, S.A. Quaiser, Angew. Chem. Int. Ed. Eng. 34 (20) (1995) 2240 (references therein).
[24] Gmelin Handbook of Inorganic Chemistry, vol. 68 C1, eighth ed., Verlag Chemie, Weinheim, 1939, p. 26.
[25] M.H. Miles, Y.H. Huang, S. Srinivasan, J. Electrochem. Soc. 125 (12) (1978) 1931.
[26] C. Iwakura, K. Fukuda, H. Tamura, Electrochim. Acta 21 (1976) 501.
[27] H.H. Kung, in: B. Delon, J.T. Yates (Eds.), Studies in Surface Science & Catalysis, Transition Metal Oxides: Surface Chemistry & Catalysis, vol. 45, Elsevier Science Publishers, 1989.
[28] J.O'M. Bockris, A.K. Reddy, Modern Electrochemistry, vol. 2, Plenum Press, New York, 1970, p. 1008 (Chapter 9).
[29] K.J. Vetter, Electrochemical Kinetics, Academic Press Inc., 1967, p. 436.
[30] D.T. Sawyer, A. Sobkowiak, J.L. Roberts Jr., Electrochemistry for Chemists, Wiley, 1995, p. 216.
[31] M.E. Orazem, J. Newman, J. Electrochem. Soc. 131 (11) (1984) 2582.
[32] N. Papageorgiou, M. Grätzel, P.P. Infelta, Sol. Energy Mater. Sol. Cells 44 (1996) 405;
N. Papageorgiou, P. Liska, A. Kay, M. Grätzel, J. Electrochem. Soc. 146 (3) (1999) 898.
[33] N. Papageorgiou, C. Barbé, M. Grätzel, J. Phys. Chem. B 102 (21) (1998) 4156.
[34] H.G. Schmidt-Weinmar, Bericht der Bunsengesellschaft, Bd. 71, Nr. 1, 1967, p. 91.
[35] Yu.A. Chizmadzhev, Yu.G. Chirkov, Comprehensive Treatise of Electrochemistry, vol. 6, Plenum Press, New York, 1983, p. 353.
[36] P.W. Atkins, Physical Chemistry, fourth ed., Oxford University Press, 1990, pp. 722–738, 761–773.
[37] N. Papageorgiou, W.F. Maier, M. Grätzel, J. Electrochem. Soc. 144 (3) (1997) 876.
[38] Stephen Wolfram, The Mathematica book, third ed., Wolfram Research Inc., 1996, pp. 818–823, 884, 1018, http:/www.wolfram.com/support/Math/Numerics/NDSolveReferences.html.
[39] N. Papageorgiou, M. Grätzel, Conference presentation at NTP3, Estes Park, USA, 1997.
[40] A. Kay, M. Grätzel, Sol. Energy Mater. Sol. Cells 44 (1996) 99.
[41] W.A. de Heer, W.S. Bacsa, A. Chatelain, T. Gerfin, R. Humphry-Baker, L. Forro, D. Ugarte, Science 268 (1995) 845.
[42] J.O'M. Bockris, A.K. Reddy, Modern Electrochemistry vol. 2, 1970, p. 1013 (Chapter 9).
[43] K. Rajeshwar, J.B. DuBow, in: Proceedings of the 16th Intersociety Energy Conversion Engineering Conference "Technologies for the Transition", The American Society of Mechanical Engineers, Atlanta, Georgia, 1981, p. 779.
[44] P. Bonhôte, A.P. Dias, N. Papageorgiou, K. Kalyanasundaram, M. Grätzel, Inorg. Chem. 35 (1996) 1168.
[45] E.I. Cooper, E.J.M. O'Sullivan, in: Proceedings of the International Symposium on Molten Salts, The Electrochemical Soc., vol. 92/6, 1992.
[46] A.T. Hubbard, F.C. Anson, in: A. Bard (Ed.), Electroanalytical Chemistry, vol. 4, 1970, p. 154.
[47] P.T. Kissinger, W.R. Heineman (Eds.), Laboratory Techniques in Electroanalytical Chemistry, Dekker, 1984.

[48] M. Grätzel, P. Liska, Photoelectrochemical cells and process for making same, U.S. Patent 5,084,365, 1992.

[49] G.E. Blomgren, in: J. Gabano (Ed.), Lithium Batteries, Academic Press, 1983, p. 19 (Chapter 2).

[50] J. Koryta, J. Dvorak, L. Kavan, Principles of Electrochemistry, Wiley, 1993, p. 120.

[51] J.O'M. Bockris, A.K. Reddy, Modern Electrochemistry, vol. 1, 1970, pp. 523–524, 547–553 (Chapter 6).

[52] K.J. Hanson, C.W. Tobias, J. Electrochem. Soc. 134 (9) (1987) 2204 (references therein).

[53] A.J. Arvia, M.C. Giordano, J.J. Podesta, Electrochim. Acta 14 (1969) 389–403.

[54] A. Bard (Ed.), Encyclopedia of Electrochemistry of the Elements, Dekker, 1973, p. 139.

[55] P.W. Atkins, Physical Chemistry, fourth ed., Oxford University Press, 1990, p. 766.

[56] H. Stegemann, A. Rohde, A. Reiche, A. Schnittke, H. Füllbier, Electrochim. Acta 37 (3) (1992) 379–383.

[57] U. Björksten, Ph.D. thesis no. 1345, Lausanne, EPFL, 1995.